



Acute lymphoblastic leukemia

Human *MLL/KMT2A* gene exhibits a second breakpoint cluster region for recurrent *MLL–USP2* fusions

Claus Meyer¹ · Bruno A. Lopes^{1,2} · Aurélie Caye-Eude³ · Hélène Cavé³ · Chloé Arfeuille³ · Wendy Cuccuini⁴ · Rosemary Sutton⁵ · Nicola C. Venn⁵ · Seung Hwan Oh^{1,6} · Grigory Tsaour⁷ · Gabriele Escherich⁸ · Tobias Feuchtinger⁹ · Hansen J. Kosasih¹⁰ · Seong L. Khaw¹⁰ · Paul G. Ekert^{5,10} · Maria S. Pombo-de-Oliveira¹¹ · Audrey Bidet¹² · Bardya Djahanschiri¹³ · Ingo Ebersberger^{13,14} · Marketa Zaliova¹⁵ · Jan Zuna¹⁵ · Zuzana Zermanova¹⁶ · Vesa Juvonen¹⁷ · Renate Panzer Grümayer¹⁸ · Grazia Fazio¹⁹ · Gianni Cazzaniga¹⁹ · Patrizia Larghero¹ · Mariana Emerenciano² · Rolf Marschalek¹

Received: 17 January 2019 / Revised: 15 February 2019 / Accepted: 8 March 2019 / Published online: 21 March 2019
© The Author(s) 2019. This article is published with open access

To the Editor:

For nearly 3 decades, the human *MLL* (*KMT2A*) gene and its rearrangements have been investigated in many different laboratories around the world. At our diagnostic center (DCAL Frankfurt), our standard strategy for the identification of *MLL-r* is based on two independent approaches, namely “Multiplex” (MP)-polymerase chain reaction (PCR) and “Long distance inverse” (LDI)-PCR approach [1]. The MP-PCR approach is used to rapidly identify the eight most frequent *MLL* fusions (*AF4*, *AF6*, *AF9*, *AF10*, *ENL*, *ELL*, *EPS15*, and *PTDs*) which encompass ~90% of all diagnosed *MLL-r* leukemia patients, while LDI-PCR is used for all other patients (~10%). By applying both technologies, we have accumulated 94 direct *MLL*-gene fusions and 247 reciprocal fusion partner genes [2]. Nearly, all breakpoints have been identified in the major breakpoint cluster region (BCR) of the *MLL* gene (*MLL* exons 8–14). However, some of the patients remained negative, although they were positively prescreened by various methods.

In order to diagnose *MLL* breakpoints in every patient, a total of 2688 overlapping Illumina capture probes covering the whole-*MLL* gene were designed and used to analyze a cohort of AL patients ($n = 109$) where we had either limited

($n = 4$; PCR positive but not sequenced) or no information ($n = 105$) on their molecular status. As depicted in Fig. 1a, we identified chromosomal rearrangements in 93 out of 109 patient cases. Sixteen patients remained *MLL-r* negative and were therefore assigned as patients with “unknown status”. The data analyses of the remaining 93 patients revealed the following distribution: for 67 patients (72%) a breakpoint could be analyzed in the major BCR; 5 patients (5%) displayed only the reciprocal *der*(TP) with breakpoints in exon 11 (putative CEP83-*MLL* spliced fusion), intron 11 ($n = 3$; putative FKBP8-*MLL* spliced fusion, *AF9-MLL*, *RELA-MLL*) and intron 27 (*IFT46-MLL*), respectively. Surprisingly, an additional 21 patients (23%) had their breakpoints outside of the major BCR, but inside a novel, minor BCR. This novel BCR is localizing between *MLL* intron 19 and exon 24 (with a clear preference for *MLL* intron 21–23).

Most of the new BCR cases represented *MLL–USP2* gene fusions ($n = 17$). *USP2* is localized about 1 Mbp telomer to *MLL* at 11q23.3 and transcriptionally orientated in direction of the centromere of chromosome 11, classifying all these fusions as intrachromosomal inversions (see Fig. 1b). In addition, we identified four balanced translocations in the minor BCR: one patient with an *USP8* fusion (see Fig. 2 and Suppl. Figure S1), two with *AF4* and one with *AF9*.

MLL–USP2 and *MLL–USP8* alleles seem to be restricted to the minor BCR (see Fig. 2), because they were never diagnosed in association with the major BCR. Most of the reciprocal *USP2–MLL* fusions were scattered over a larger region at 11q23.3 (see Fig. 2), involving also upstream (*C2CD2L*) and downstream genes (*USP2-AS1*). Our analysis revealed also five patients with 3′-*MLL* deletions that were caused by microdeletions (<200 bp), larger deletions (up to 34 kbp), or complex rearrangements including other

These authors contributed equally: Claus Meyer, Bruno A. Lopes

Supplementary information The online version of this article (<https://doi.org/10.1038/s41375-019-0451-7>) contains supplementary material, which is available to authorized users.

✉ Rolf Marschalek
rolf.marschalek@em.uni-frankfurt.de

Extended author information available on the last page of the article

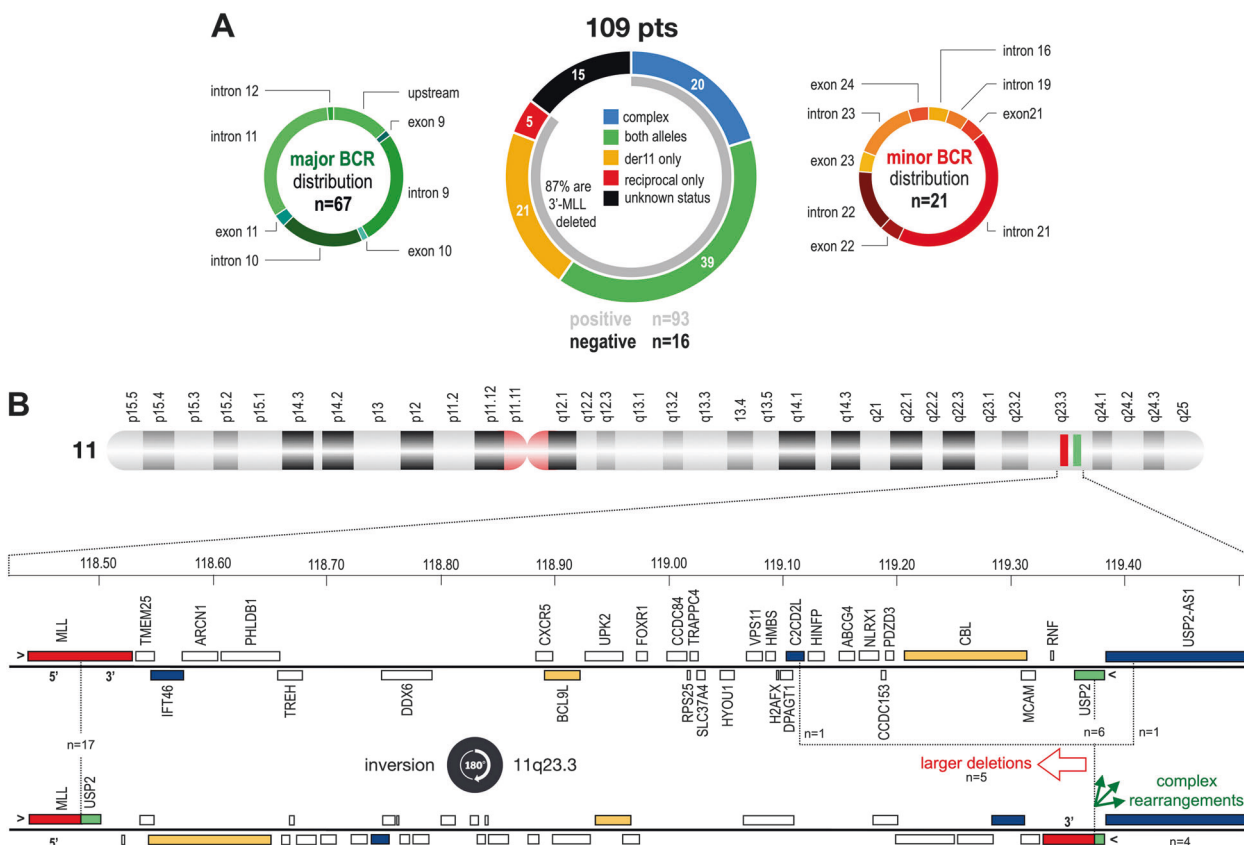


Fig. 1 Overview about all analyzed patients, their molecular information and breakpoint distribution. **a** Data from 109 patients which were analyzed with NGS in percentages. Their breakpoint distribution is displayed left (major BCR; $n = 67$) and right (minor BCR; $n = 21$). Five patients displayed only a reciprocal fusion, while 16 cases displayed no *MLL* rearrangement. **b** Top: chromosome 11 is depicted with highlighting of the *MLL* (red) and *USP2* (green) genes. Below: all

the genes between *MLL* and *USP*; blue marked genes: additional genes found in this study to be rearranged with *MLL*; orange marked genes: genes that have been earlier described to be rearranged with *MLL*. Recombinations between *MLL* and *USP2* are caused by an inversion, with reciprocal alleles that carry additional deletions or complex rearrangements

chromosomes as well ($n = 4$; chromosome regions 2p21, 4q13.1, 12p13.33, and 18p11.32). A detailed picture of the investigated *MLL-USP2* and *MLL-USP8* and their reciprocal fusions is shown in the Suppl. Fig. S2A–D.

All patients with a rearrangement of *USP2* or *USP8* fused the conserved “UCH-domain” to an extended 5'-*MLL* portion (see Suppl. Fig. S1A). This may indicate that the UCH domain has a functional importance for the resulting *MLL* fusion protein. *USP* genes belong to a large group of deubiquitinating proteins binding to specific target proteins [3–5]. The *USP* family exhibits a ubiquitin-specific protease (UCH domain) that is characterized by several conserved amino acids that are summarized as CYS- and ASP-box (see Suppl. Fig. 1B). *USP2* protein deubiquitinates and stabilizes MDM2, leading to an enhanced degradation of p53 [6]. This in turn activates MYC, because active p53 induces the transcription of several microRNAs that target MYC mRNA.

MLL fusions with the conserved 3'-UCH domain of *USP2* and *USP8* may change profoundly the functions of

these novel *MLL* fusion proteins. It has already been shown that PHD2 [7] and PHD3/BD [8] both bind to proteins (CDC34 and ESC^{ASB2}) that mediate the destruction of *MLL* by poly-ubiquitination and proteasomal degradation. Fusing single or all PHD domains to a der(11) product (*MLL-AF9* and *MLL-ENL*) caused even a strong drop of their transforming potential [9, 10]. This well-described degradation mechanism of *MLL* may now be counteracted by the UCH domain of *MLL-USP2* or *MLL-USP8*, and thus, restoring their oncogenic transformation capacity.

In our cohort, we also identified new *MLL* fusion partner genes ($n = 3$). These novel fusion genes were *SNX9* (6q25.3), *USP8* (15q21.2), and *SEPT3* (22q13.2). *SNX9* encodes a protein known to be a member of the sorting nexin family which contain a phosphoinositide binding domain and are involved in intracellular trafficking. The *SNX9* protein has a variety of interaction partners, including an adapter protein 2, dynamin, tyrosine kinase non-receptor 2, Wiskott–Aldrich syndrome-like, and ARP3 actin-related protein 3. *USP8* has diverse functions, being

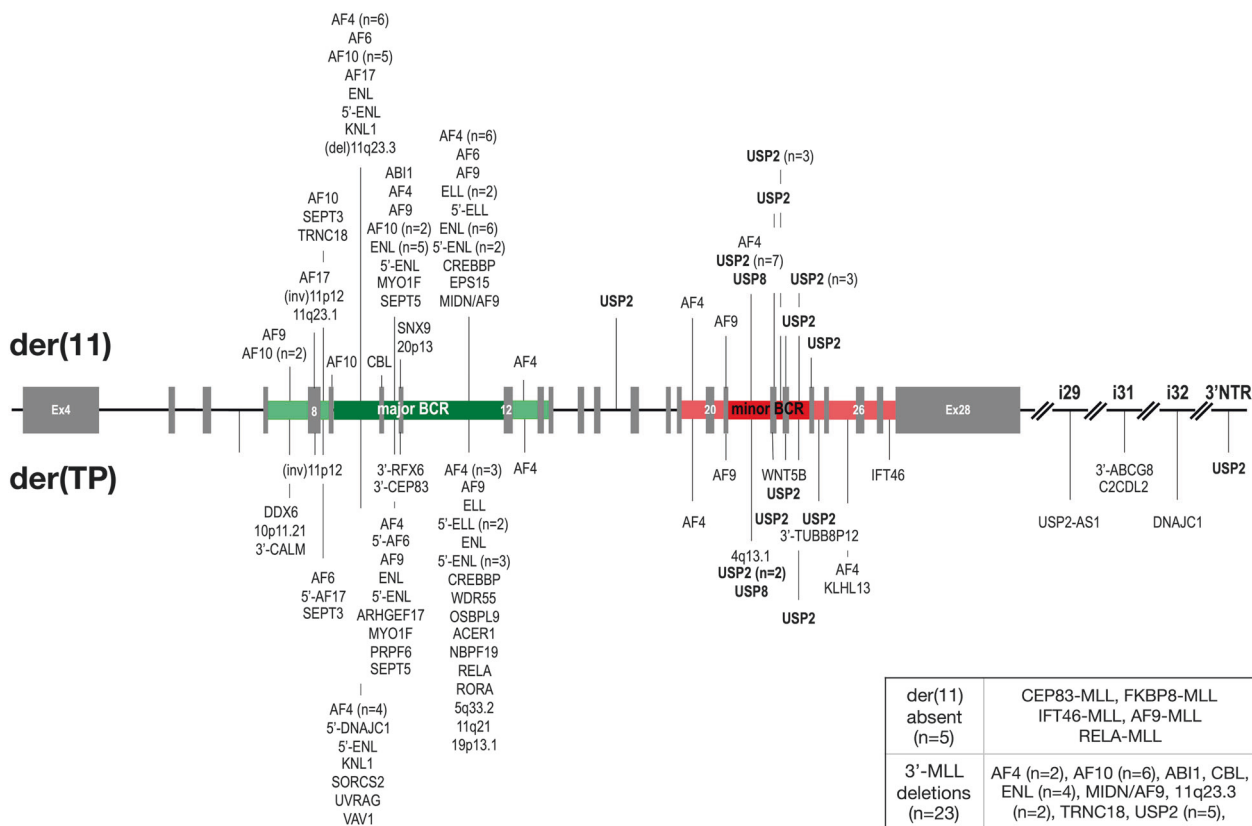


Fig. 2 Detailed distribution of all breakpoints in both BCRs of *MLL*. The *MLL* gene is depicted from exon 4 to the end. The major BCR is marked in green, the minor BCR in red. Main breakpoint regions are depicted in dark green/red while regions with fewer breakpoints are

depicted in light green/red. The fusions sites and the fusion partners are shown. Information about the 5 cases with no der(11) or the 23 cases with 3'-*MLL* deletions are given in the box at the right bottom

required for the internalization of liganded receptor tyrosine kinases and stabilization of ESCRT components. The *USP8* protein is thought to regulate the morphology of the endosome by ubiquitination of proteins on this organelle and is involved in cargo sorting and membrane trafficking at the early endosome stage. *SEPT3* is the seventh member of the septin family of GTPases that is fused to *MLL*. Members of this family are required for cytokinesis.

A few cases of *MLL-USP2* fusions have already been described. However, these were single patient cases and they were classified as exceptional rearrangements [11–13]. Our NGS approach allowed for the first time the recurrent characterization of breakpoints in this novel minor BCR region of the *MLL* gene. Moreover, our targeted NGS approach enabled us to overcome the technical limitations associated with LDI-PCR and MP-PCR approaches.

Another advantage of the targeted NGS approach is the simultaneous identification of 3' *MLL* deletions or copy number variations. In the current study, 23 of the patients (out of 88: 26%) had a 3' *MLL* deletion. According to our data, 3'-*MLL* deletions were present in both breakpoint groups (major and minor) to a similar extent with 26.9% and 23.8%, respectively. This seems to be much higher than

previously described (Andersson et al. [12]: 13%; Peterson et al. [14]: 7%).

In diagnostic fluorescence in situ hybridization analyses, these *MLL-USP2* cases revealed two major patterns: (1) loss of the 3'-*MLL* probe signal, and (2) a normal pattern typical for *MLL* wild-type (Suppl. Table S1b, Suppl. Fig. S3). Considering the clinical data (Suppl. Table S1a–c), our 17 patients with *MLL-USP2* were divided into 8 males and 9 females. All of them were children, and the median age at diagnosis was 17 months (range: 3–120 months). The median leukocyte count was $30.4 \times 10^9/L$ (range: $3.4\text{--}324.0 \times 10^9/L$), and the disease phenotype was predominantly B-ALL ($n = 12$), followed by mixed-phenotype acute leukemia (MPAL) ($n = 4$) and acute myeloid leukemia ($n = 1$). The MPAL cases all had mixed myeloid and B-cell phenotype. The patients were treated with diverse therapy protocols. Five patients (29%) presented with central nervous system disease, and 13 patients (76%) had positive-minimal residual disease (MRD) levels at day 33. Prednisone response was measured in 12 patients with a poor response in 5 patients (42%). The median follow-up of the patients was 1.2 years (range: 0.1–11.1 years), and 2 cases died after 5 and 9 months following

diagnosis. The remaining patients are still at first clinical remission.

In conclusion, we have identified a minor BCR within the human *MLL* gene that is recurrently associated in acute leukemia patients with *MLL-USP2* fusion alleles as well as *MLL* fusion partnerships with *USP8*, *AF4*, and *AF9*. However, with 17 cases out of ~2500 analyzed patients the incidence is less than 1% while still ranking fourteenth of our updated fusion gene list (see Table 1 of reference 1). The discovery of a second, minor BCR extends our knowledge of the *MLL*-recombinome and *MLL*-r oncogenesis. Moreover, these findings will enable many labs to make changes in their diagnostic set-up for *MLL*-MRD diagnostics to ensure the best medical treatment for a group of patients that is still very hard to cure.

Acknowledgements BAL received a fellowship provided by CAPES and the Alexander von Humboldt Foundation (#88881.136091/2017-01). ME is supported by CNPq (PQ-2017#305529/2017-0) and FAPERJ-JCNE (#26/203.214/2017) research scholarships, and ZZ by grant RVO-VFN64165. GC is supported by the AIRC Investigator grant IG2015 grant no. 17593 and RS by Cancer Australia grant PdCCRS1128727. This work was supported by grants to RM from the “Georg und Franziska Speyer’sche Hochschulstiftung”, the “Wilhelm Sander foundation” (grant 2018.070.1) and DFG grant MA 1876/12-1.

Compliance with ethical standards

Conflict of interest The authors declare that they have no conflict of interest.

Publisher’s note: Springer Nature remains neutral with regard to jurisdictional claims in published maps and institutional affiliations.

Open Access This article is licensed under a Creative Commons Attribution 4.0 International License, which permits use, sharing, adaptation, distribution and reproduction in any medium or format, as long as you give appropriate credit to the original author(s) and the source, provide a link to the Creative Commons license, and indicate if changes were made. The images or other third party material in this article are included in the article’s Creative Commons license, unless indicated otherwise in a credit line to the material. If material is not included in the article’s Creative Commons license and your intended use is not permitted by statutory regulation or exceeds the permitted use, you will need to obtain permission directly from the copyright holder. To view a copy of this license, visit <http://creativecommons.org/licenses/by/4.0/>.

Affiliations

Claus Meyer¹ · Bruno A. Lopes^{1,2} · Aurélie Caye-Eude³ · Hélène Cavé³ · Chloé Arfeuille³ · Wendy Cuccini⁴ · Rosemary Sutton⁵ · Nicola C. Venn⁵ · Seung Hwan Oh^{1,6} · Grigory Tsaur⁷ · Gabriele Escherich⁸ · Tobias Feuchtinger⁹ · Hansen J. Kosasih¹⁰ · Seong L. Khaw¹⁰ · Paul G. Ekert^{5,10} · Maria S. Pombo-de-Oliveira¹¹ · Audrey Bidet¹² · Bardya Djahanschiri¹³ · Ingo Ebersberger^{13,14} · Marketa Zaliova¹⁵ · Jan Zuna¹⁵ · Zuzana Zermanova¹⁶ · Vesa Juvonen¹⁷ · Renate Panzer Grümayer¹⁸ · Grazia Fazio¹⁹ · Gianni Cazzaniga¹⁹ · Patrizia Larghero¹ · Mariana Emerenciano¹⁹ · Rolf Marschalek¹⁹

References

- Meyer C, Schneider B, Reichel M, Angermueller S, Strehl S, Schnitger S, et al. Diagnostic tool for the identification of *MLL* rearrangements including unknown partner genes. *Proc Natl Acad Sci USA*. 2005;102:449–54.
- Meyer C, Burmeister T, Gröger D, Tsaur G, Fehina L, Renneville A, et al. The *MLL* recombinome of acute leukemias in 2017. *Leukemia*. 2018;32:273–84.
- Zhang W, Sulea T, Tao L, Cui Q, Purisima EO, Vongsamphanh R, et al. Contribution of active site residues to substrate hydrolysis by *USP2*: insights into catalysis by ubiquitin specific proteases. *Biochemistry*. 2011;50:4775–85.
- Nishi R, Wijnhoven P, le Sage C, Tjeertes J, Galanty Y, Forment JV, et al. Systematic characterization of deubiquitylating enzymes for roles in maintaining genome integrity. *Nat Cell Biol*. 2014;16:1016–26.
- Clague MJ, Barsukov I, Coulson JM, Liu H, Rigden DJ, Urbé S. Deubiquitylases from genes to organism. *Physiol Rev*. 2013;93:1289–315.
- Sacco JJ, Coulson JM, Clague MJ, Urbé S. Emerging roles of deubiquitinases in cancer-associated pathways. *IUBMB Life*. 2010;62:140–57.
- Wang J, Muntean AG, Hess JL. ECSASB2 mediates *MLL* degradation during hematopoietic differentiation. *Blood*. 2012a;119:1151–61.
- Wang J, Muntean AG, Wu L, Hess JL. A subset of mixed lineage leukemia proteins has plant homeodomain (PHD)-mediated E3 ligase activity. *J Biol Chem*. 2012b;287:43410–6.
- Muntean AG, Giannola D, Udager AM, Hess JL. The PHD fingers of *MLL* block *MLL* fusion protein-mediated transformation. *Blood*. 2008;112:4690–3.
- Chen J, Santillan DA, Koonce M, Wei W, Luo R, Thirman MJ, et al. Loss of *MLL* PHD finger 3 is necessary for *MLL*-*ENL*-induced hematopoietic stem cell immortalization. *Cancer Res*. 2008;68:6199–207.
- Roberts KG, Li Y, Payne-Turner D, Harvey RC, Yang YL, Pei D, et al. Targetable kinase-activating lesions in Ph-like acute lymphoblastic leukemia. *N Engl J Med*. 2014;371:1005–15.
- Andersson AK, Ma J, Wang J, Chen X, Gedman AL, Dang J, et al. St. Jude Children’s Research Hospital–Washington University Pediatric Cancer Genome Project. The genetic basis and cell of origin of mixed phenotype acute leukaemia. The landscape of somatic mutations in infant *MLL*-rearranged acute lymphoblastic leukemias. *Nat Genet*. 2015;47:330–7.
- Alexander TB, Gu Z, Iacobucci I, Dickerson K, Choi JK, Xu B, et al. The genetic basis and cell of origin of mixed phenotype acute leukaemia. *Nature*. 2018;562:373–9.
- Peterson JF, Baughn LB, Pearce KE, Williamson CM, Benevides Demasi JC, Olson RM, et al. *KMT2A* (*MLL*) rearrangements observed in pediatric/young adult T-lymphoblastic leukemia/lymphoma: A 10-year review from a single cytogenetic laboratory. *Genes Chromosomes Cancer*. 2018;57:541–6.

- ¹ DCAL/Institute of Pharmaceutical Biology, Goethe-University Frankfurt, Frankfurt am Main, Germany
- ² Division of Clinical Research, Research Center, Instituto Nacional de Cancer, Rio de Janeiro, Brazil
- ³ Department of Genetics, AP-HP Robert Debré, Paris Diderot University, Paris, France
- ⁴ Department of Cytogenetics, Saint Louis Hospital, Paris, France
- ⁵ Children's Cancer Institute Australia, University of NSW Sydney, Sydney, Australia
- ⁶ Department of Laboratory Medicine, Inje University College of Medicine, Busan, Korea
- ⁷ Regional Children Hospital 1, Research Institute of Medical Cell Technologies, Pediatric Oncology and Hematology Center, Ural Federal University named after the first President of Russia BN Yeltsin, Ekaterinburg, Russia
- ⁸ Clinic of Pediatric Hematology and Oncology, University Medical Center Hamburg-Eppendorf, Hamburg, Germany
- ⁹ Department of Pediatric Hematology, Oncology, Hemostaseology and Stem Cell Transplantation, Dr. von Hauner University Children's Hospital, Ludwig Maximilian University Munich, Munich, Germany
- ¹⁰ Murdoch Children's Research Institute, The Royal Children's Hospital, Flemington Road Parkville, 3052 Victoria, Australia
- ¹¹ Pediatric Hematology-Oncology Program—Research Center, Instituto Nacional de Cancer Rio de Janeiro, Rio de Janeiro, Brazil
- ¹² Laboratoire d'Hématologie, University Hospital, Brest, CHU de Bordeaux, Bordeaux, France
- ¹³ Department of Applied Bioinformatics, Institute of Cell Biology and Neuroscience, Goethe-Universität Frankfurt, Frankfurt am Main 60438, Germany
- ¹⁴ Senckenberg Climate and Research Centre (BIK-F), Frankfurt am Main 60325, Germany
- ¹⁵ CLIP, Department of Paediatric Haematology/Oncology, Charles University Prague, 2nd Faculty of Medicine, Prague, Czech Republic
- ¹⁶ Center of Oncocytogenetics, Institute of Medical Biochemistry and Laboratory Diagnostics, General University Hospital and First Faculty of Medicine, Charles University, Prague, Czech Republic
- ¹⁷ Department of Clinical Chemistry and Laboratory Division, Turku University Hospital, Turku, Finland
- ¹⁸ Children's Cancer Research Institute, Medical University of Vienna, Vienna, Austria
- ¹⁹ Centro Ricerca Tettamanti, Clinica Pediatrica University of Milano-Bicocca, Monza, Italy

Leukemia (2019) 33:2310–2314

<https://doi.org/10.1038/s41375-019-0465-1>

Animal models

FLT3^{N676K} drives acute myeloid leukemia in a xenograft model of *KMT2A-MLL3* leukemogenesis

Axel Hyrenius-Wittsten ¹ · Mattias Pilheden¹ · Antoni Falqués-Costa¹ · Mia Eriksson¹ · Helena Stuesson¹ · Pauline Schneider² · Priscilla Wander² · Cristian Garcia-Ruiz ¹ · Jian Liu¹ · Helena Ågerstam¹ · Anne Hultquist^{3,4} · Henrik Lilljebjörn ¹ · Ronald W. Stam² · Marcus Järås¹ · Anna K. Hagström-Andersson ¹

Received: 6 December 2018 / Revised: 1 March 2019 / Accepted: 22 March 2019 / Published online: 5 April 2019

© The Author(s) 2019. This article is published with open access

Supplementary information The online version of this article (<https://doi.org/10.1038/s41375-019-0465-1>) contains supplementary material, which is available to authorized users.

✉ Anna K. Hagström-Andersson
Anna.Hagstrom@med.lu.se

- ¹ Division of Clinical Genetics, Department of Laboratory Medicine, Lund University, Lund, Sweden
- ² Princess Máxima Center for Pediatric Oncology, Utrecht, The Netherlands
- ³ Department of Pathology, Skane University Hospital, Lund University, Lund, Sweden
- ⁴ Lund Stem Cell Center, Lund University, Lund, Sweden

To the Editor:

Activating signaling mutations are common in acute leukemia with *KMT2A* (previously *MLL*) rearrangements (*KMT2A-R*) [1]. When defining the genetic landscape of infant *KMT2A-R* acute lymphoblastic leukemia (ALL), we identified a novel *FLT3*^{N676K} mutation in both infant ALL and non-infant acute myeloid leukemia (AML) [1]. *FLT3*^{N676K} was the most common *FLT3* mutation in our cohort and we recently showed that it cooperates with *KMT2A-MLL3* in a syngeneic mouse model [1, 2]. To study the ability of *FLT3*^{N676K} to cooperate with *KMT2A-MLL3* in human leukemogenesis, we transduced human

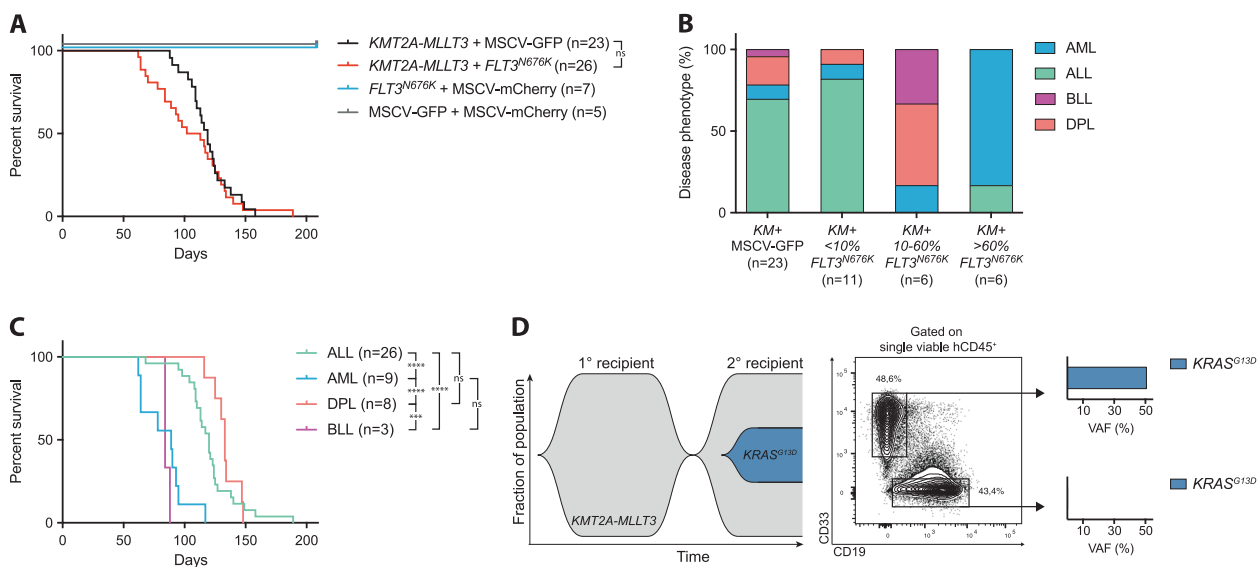


Fig. 1 *FLT3*^{N676K} alters the lineage distribution of *KMT2A-MLL3*-driven leukemia. **a** Kaplan–Meier survival curves of NSG mice transplanted with CD34⁺ cord blood cells cotransduced with *KMT2A-MLL3* + *FLT3*^{N676K} ($n = 23$), *KMT2A-MLL3* + MSCV-GFP ($n = 26$, of which three died and no tissue samples could be collected), *FLT3*^{N676K} + MSCV-mCherry ($n = 7$), or MSCV-GFP + MSCV-mCherry ($n = 5$). **b** Distribution of mice that succumbed to ALL, AML, DPL, or BLL within *KMT2A-MLL3* + MSCV-GFP and *KMT2A-MLL3*-mCherry + *FLT3*^{N676K}-GFP recipients divided on the fraction of mCherry⁺GFP⁺ (<10%, $n = 11$; 10–60%, $n = 6$; or >60%, $n = 6$) cells within hCD45⁺ bone marrow (BM) cells. **c** Kaplan–Meier

survival curves of all xenograft leukemias based on their immunophenotype showed an accelerated disease for AML as compared with both ALL ($P < 0.0001$) and DPL ($P < 0.0001$). **d** Fish plot showing progression of one *KMT2A-MLL3* + MSCV-GFP BLL that gained a *de novo* *KRAS*^{G13D} (VAF 17% in hCD45⁺ BM cells) in the secondary recipient (h11.13-1) and targeted resequencing of hCD45⁺ CD19⁻CD33⁺ and hCD45⁺CD19⁺CD33⁻ BM cells from the secondary recipient (h11.13-1) revealed the *KRAS*^{G13D} mutation to reside in CD19⁻CD33⁺ leukemia cells (VAF 51%). Mantel–Cox log-rank test, *** $P \leq 0.001$, **** $P \leq 0.0001$, ns = not significant

CD34⁺-enriched cord blood (CB) cells and followed leukemia development immunophenotypically and molecularly in NOD.Cg-*Prkdc*^{scid}*Ii2rg*^{tm1Wjl}/SzJ (NSG) mice.

Mice that received *KMT2A-MLL3* with or without *FLT3*^{N676K} developed a lethal leukemia, often with splenomegaly, thrombocytopenia, and leukocytosis, with no difference in median disease latency (107.5 and 119 days, respectively, $P = 0.48$) and mice receiving *FLT3*^{N676K} alone showed no sign of disease (Fig. 1a, Supplementary Fig. 1A–E, and Supplementary Data 1). Leukemic mice succumbed to ALL (>50% CD19⁺CD33⁻), AML (>50% CD19⁻CD33⁺), double-positive leukemia (DPL, >20% CD19⁺CD33⁺), or bilineal leukemia (BLL, <50% CD19⁺CD33⁻, <50% CD19⁻CD33⁺, and <20% CD19⁺CD33⁺); thus, the leukemias often coexisted with leukemia cells of another immunophenotype (Supplementary Fig. 1F, G and Supplementary Data 1) [3–5]. Previous studies have shown that retroviral overexpression of *KMT2A-MLL3* in human CB cells in NOD.CB17/*Prkdc*^{scid} (NOD/SCID), NOD.Cg-*Prkdc*^{scid}*B2m*^{tm1Unc} (NOD/SCID-B2m), or NSG immunodeficient mice, primarily gives rise to ALL, sometimes to leukemias expressing both lymphoid and myeloid markers or bilineal leukemias, but rarely AML [3–6]. *KMT2A-MLL3*-driven AML can only be generated with high penetrance, and retransplanted in immunodeficient mice transgenically expressing human myeloid cytokines, consistent with the idea that

external factors can influence the phenotype of the developing leukemia [3, 6]. In agreement, most recipients that received *KMT2A-MLL3* alone developed ALL (16/23, 69.6%) or DPL (4/23, 17.4%) and AML was rare (2/23, 8.7%) [3, 4, 6]. By contrast, five out of six recipients that received *KMT2A-MLL3*+*FLT3*^{N676K} and that had >60% ($n = 6$, range 60.4–94.1%) of co-expressing cells, developed AML and one developed ALL (Fig. 1b, Supplementary Fig. 1H, I, and Supplementary Data 1). Thus, *FLT3*^{N676K} preferentially drives myeloid expansion, similar to mutant *Flt3* in a syngeneic setting [7]. *FLT3* is expressed in human hematopoietic stem and progenitor cells, with the highest expression in granulocyte–macrophage progenitors (GMPs), and its signaling supports survival of those cells [8]. Combined, this suggests that *FLT3*^{N676K} affects the survival of myeloid progenitors. In this context, it is interesting to note that *FLT3* tyrosine kinase domain mutations are enriched in pediatric AML with *KMT2A-MLL3* [9, 10]. Most recipients with <10% ($n = 11$, range 0.2–5.3%) of co-expressing *KMT2A-MLL3* + *FLT3*^{N676K} cells succumbed to ALL, consistent with leukemia being driven by *KMT2A-MLL3* alone. Among those with 10–60% ($n = 6$, range 10.9–31.6%) of co-expressing cells, a mixture of diseases developed since leukemia could be driven both by *KMT2A-MLL3* alone and *KMT2A-MLL3* + *FLT3*^{N676K} (Fig. 1b, Supplementary Fig. 1H, I, and Supplementary Data 1).

Co-expression of *KMT2A-MLLT3* and *FLT3^{N676K}* preferentially expanded myeloid cells ($P < 0.0001$, Supplementary Fig. 1J) and a high proportion of $CD19^-CD33^+$ cells at sacrifice, across the cohort, correlated with accelerated disease ($r_s = -0.6537$, $P < 0.0001$, Supplementary Fig. 1K, L). In agreement, AML developed with significantly shorter latency as compared with ALL and DPL (89 vs. 120 and 133 days, respectively, both $P < 0.0001$), but not with BLL (84 days, Fig. 1c). Further, *FLT3^{N676K}*-driven AML had a tendency toward shorter survival (median latency 78 days, range 62–117 days vs. 93 days for *KMT2A-MLLT3* alone, Supplementary Data 1).

To determine the evolution of phenotypically distinct leukemia cells in secondary recipients, BM cells from six primary *KMT2A-MLLT3* + *FLT3^{N676K}* leukemias (three each with $> 60\%$ or 20–32% of *FLT3^{N676K}*-expressing cells) and from four primary *KMT2A-MLLT3* leukemias, were retransplanted. All leukemias gave rise to secondary malignancies and recipients that received BM from AML ($n = 2$) and ALL ($n = 1$) with $> 60\%$ of *KMT2A-MLLT3* + *FLT3^{N676K}* cells had an accelerated disease onset and maintained leukemia immunophenotype (median latency of 117 and 41 days, for the primary and secondary recipients, respectively) (Supplementary Fig. 2A–E and Supplementary Data 2). Thus, *FLT3^{N676K}* circumvented the cytokine dependence normally required for myeloid cells in immunodeficient mice [3]. By contrast, all secondary recipients that received BM with 20–32% *KMT2A-MLLT3* + *FLT3^{N676K}* cells succumbed to ALL, irrespective of disease phenotype in the primary recipients (one AML and two BLL). Thus, the myeloid *FLT3^{N676K}*-expressing cells unexpectedly decreased in size, while the *KMT2A-MLLT3*-expressing lymphoid cells increased to clonal dominance (Supplementary Fig. 2F, G and Supplementary Data 2). This suggests that the *FLT3^{N676K}*-containing myeloid leukemia population needs to be sufficiently large to expand in secondary recipients, either because they otherwise are out-competed by the larger population of more easily engrafted ALL cells, or because they themselves need to mediate the permissive microenvironment that allows myeloid cells to engraft. Similarly, in all but one of the secondary recipients that received BM from leukemias expressing only *KMT2A-MLLT3* (two AML, one ALL, and one BLL), the disease phenotype changed and myeloid cells did not engraft (Supplementary Fig. 2H–J and Supplementary Data 2).

In the secondary recipient with maintained immunophenotype (a BLL, h11.13-1), the myeloid cells unexpectedly expanded from 38% to close to 50% (Fig. 1d and Supplementary Data 2). This suggested that the myeloid cells had acquired a de novo mutation that allowed serial transplantation, similar to what was observed for *FLT3^{N676K}*. Strikingly, targeted sequencing of AML-associated genes on $hCD45^+$ BM from this mouse

identified a *KRAS^{G13D}* in 34% of the cells. Resequencing of $hCD45^+CD19^-CD33^+$ and $hCD45^+CD19^+CD33^-$ BM showed that *KRAS^{G13D}* was present exclusively in the myeloid population and based on the variant allele frequency of 51%, that all cells carried the mutation (Fig. 1d and Supplementary Table 1, 2). Further, *KRAS^{G13D}* likely arose independently in h11.13-1 as no mutation was identified, at the level of our detection, in the primary (h11.13) or in a separate secondary recipient (h11.13-2) from the same primary mouse (h11.13) that developed ALL (Supplementary Table 2 and Supplementary Data 2).

Gene expression profiling (GEP) followed by principal component analysis (PCA) showed that the leukemias segregated based on their immunophenotype, with an evident separation between leukemias and normal hematopoietic cells (Fig. 2a, Supplementary Fig. 3A, B, and Supplementary Table 3). All leukemias expressed high levels of known *KMT2A-R* target genes and showed enrichment of gene signatures associated with primary *KMT2A-R* leukemia, indicating that they maintain a GEP representative of human disease (Supplementary Fig. 3C, D and Supplementary Data 3–6). In line with the hypothesis that *KMT2A-MLLT3* DPL cells are ALL cells with aberrant CD33 expression, they clustered closely with ALL cells. Both populations expressed high levels of ALL-associated cell surface markers and lymphoid transcription factors (Fig. 2a and Supplementary Fig. 3B, E–H). Further, *CD33* and other AML-associated cell surface markers and key myeloid transcription factors, all showed lower expression in DPL cells as compared with normal myeloid- and AML cells (Supplementary Fig. 3G–I).

By correlating the GEPs of the xenograft leukemias to those of normal hematopoietic cells [11], DPL and ALL were found to resemble normal common lymphoid progenitors (CLPs) and AML cells normal GMPs (Fig. 2b). Further, ALL and DPL cells had significantly higher expression of the transcription factor *CEBPA* as compared with normal lymphoid cells which lacked *CEBPA* expression (Fig. 2c). *CEBPA* drives myeloid programs and is expressed in most hematopoietic progenitors, in particular in GMPs, with CLPs lacking *CEBPA* expression (Fig. 2c) [11]. Finally, to link the GEPs of our xenograft leukemias to those of pediatric *KMT2A-R* leukemia, we utilized a dataset of pediatric B-cell precursor ALL (BCP-ALL) [12]. Multigroup comparison visualized by PCA showed that *KMT2A-MLLT3* DPL and ALL mainly resembled *KMT2A-R* BCP-ALL (Fig. 2d), again highlighting that the xenograft leukemias resemble human leukemia.

We next studied the transcriptional changes induced by *FLT3^{N676K}* in *KMT2A-MLLT3* AML cells. Gene set enrichment analysis (GSEA) revealed enrichment of gene sets connected to the Myc-transcriptional network, cell

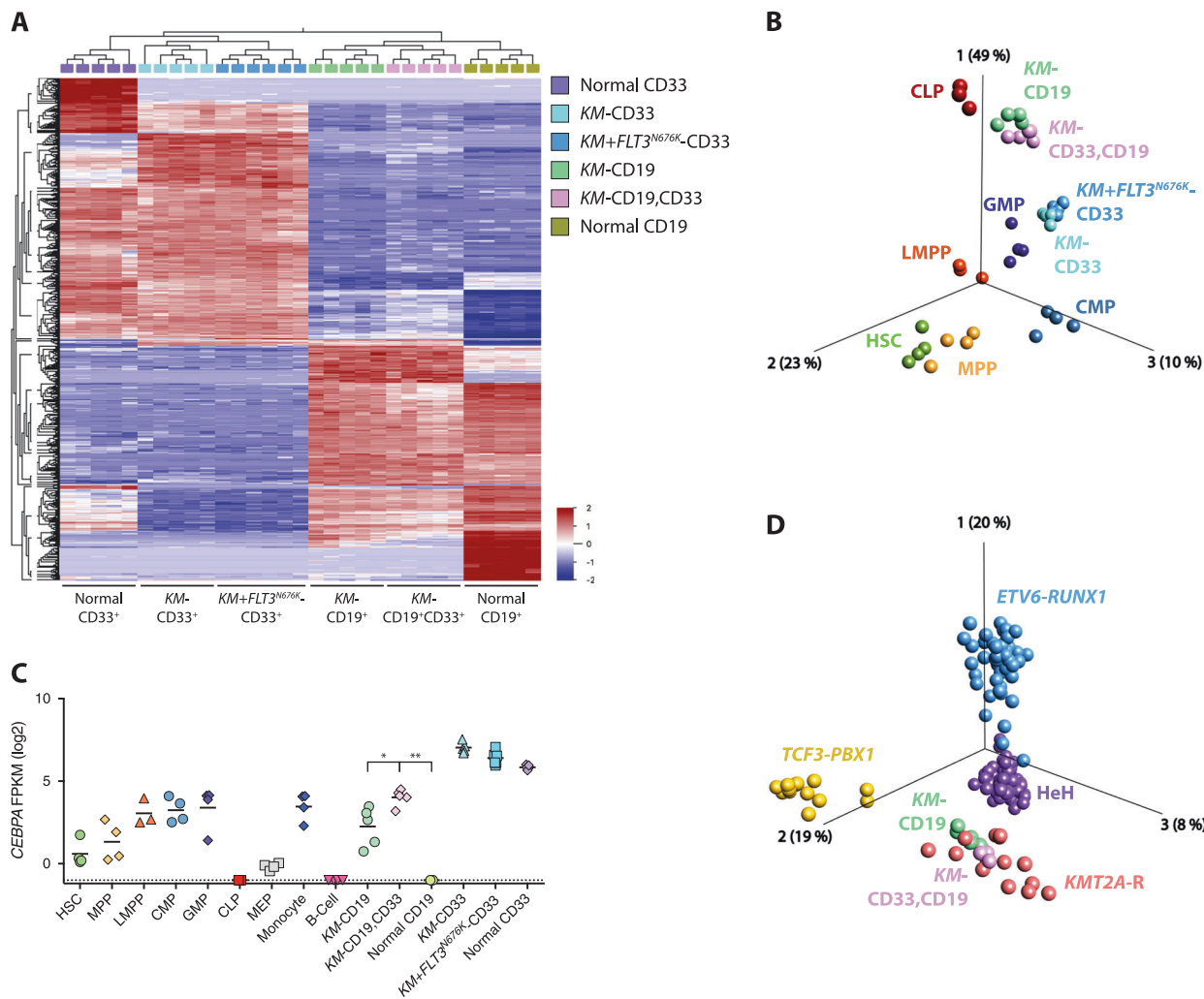


Fig. 2 DPL cells are ALL cells with aberrant CD33 expression. **a** Hierarchical clustering based on multigroup comparison of myeloid CD19⁻CD33⁺ leukemia cells from *KMT2A-MLL3* + MSCV-GFP (*KM-CD33*) and *KMT2A-MLL3* + *FLT3*^{N676K} (*KM + FLT3*^{N676K}-CD33), lymphoid CD19⁺CD33⁻ leukemia cells from *KMT2A-MLL3* + MSCV-GFP (*KM-CD19*), and double-positive CD19⁺CD33⁺ leukemia cells from *KMT2A-MLL3* + MSCV-GFP (*KM-CD19,CD33*), as well as normal myeloid- CD19⁻CD33⁺ (normal CD33) and lymphoid CD19⁺CD33⁻ (normal CD19) cells from MSCV-GFP + MSCV-mCherry using 637 variables ($P = 2.2e^{-15}$, FDR = $4.9e^{-14}$). **b** Supervised (1500 variables, $P = 3.6e^{-4}$, FDR = $3.1e^{-3}$) PCA based on human hematopoietic stem cells (HSC), multipotent progenitors (MPP), lymphoid-primed multipotent progenitors (LMPP), common myeloid progenitors (CMP), granulocyte-

macrophage progenitors (GMP), and common lymphoid progenitors (CLP) [11]. Samples with leukemia cells from *KM-CD33*, *KM + FLT3*^{N676K}-CD33, *KM-CD19*, and *KM-CD19,CD33* were inserted into the same PCA (still based solely on the normal populations [11]), revealing that AML cells mainly resembled GMPs and that both ALL and DPL mainly resembled CLPs. **c** *CEBPA* expression (FPKM log2) within sorted leukemia, normal populations, and within HSC, MPP, LMPP, CMP, GMP, CLP, MEP, monocytes, and B cells [11]. **d** Supervised (1501 variables, $P = 3.3e^{-10}$, FDR = $3.1e^{-9}$) PCA based on pediatric BCP-ALL with *ETV6-RUNX1*, high hyperdiploid (HeH), *TCF3-PBX1*, or *KMT2A-R* [12]. Samples with leukemia cells from *KM-CD19* and *KM-CD19,CD33* were inserted into the same PCA (still based solely on the pediatric BCP-ALL populations [12]). Mann-Whitney U test used in (c), * $P \leq 0.05$, ** $P \leq 0.01$, ns = not significant

cycle, and proliferation when compared with *KMT2A-MLL3* AML (Supplementary Data 7). Similar to our previous findings in a syngeneic *KMT2A-MLL3* mouse model [2], the Myc-centered program [13] was not linked to the pluripotency network (Supplementary Fig. 4A and Supplementary Data 8, 9). Since *FLT3* mutations activate mitogen-activated protein kinase (MAPK) signaling [14], we investigated if *FLT3*^{N676K} increased expression of MEK/ERK-pathway genes, by studying the expression of known

transcriptional output genes and negative feedback regulators of the pathway [15]. Indeed, enrichment of MEK/ERK-associated genes was evident in *FLT3*^{N676K}-expressing cells, suggesting that *FLT3*^{N676K} allows cells to overcome normal feedback regulation, leading to sustained signaling [15] (Supplementary Fig. 4B). Finally, *FLT3*^{N676K}-expressing AML showed preserved transcriptional changes to those seen in infant *KMT2A-AFF1* ALL with activating mutations [1] (Supplementary Fig. 4C). Thus, *FLT3*^{N676K}

may circumvent the cytokine dependence seen for myeloid cells in immunodeficient mice by providing constitutive active signaling promoting cell proliferation, likely through the MAPK/ERK pathway.

Herein, we demonstrate that co-expression of *KMT2A-MLLT3* and *FLT3^{N676K}* in human CB cells primarily causes AML and thus alters the lineage distribution of *KMT2A-MLLT3*-driven leukemia. AML could only be serially transplanted with maintained immunophenotype in the presence of *FLT3^{N676K}*. This is consistent with the idea that activated signaling allows myeloid cells to more efficiently engraft and maintain their self-renewal. In agreement, we identified a *de novo* *KRAS^{G13D}* in myeloid *KMT2A-MLLT3*-expressing cells that had expanded upon secondary transplantation. Altogether, this shows that constitutively active signaling mutations can substitute for external factors and influence the phenotype of the developing *KMT2A-R* leukemia, at least in xenograft models.

Accession code

GSE127492.

Acknowledgements This work was supported by The Swedish Childhood Cancer Foundation, The Swedish Cancer Society, The Swedish Research Council, The Knut and Alice Wallenberg Foundation, BioCARE, The Crafoord Foundation, The Per-Eric and Ulla Schyberg Foundation, The Nilsson-Ehle Donations, The Wiberg Foundation, and Governmental Funding of Clinical Research within the National Health Service. Work performed at the Center for Translational Genomics, Lund University has been funded by Medical Faculty Lund University, Region Skåne and Science for Life Laboratory, Sweden.

Author contributions AHW and AKHA designed the study and experiments; AHW, MP, AFC, ME, HS, PS, PW, CGR, JL, and HÅ performed experiments; AHW, MP, HL, and AKHA analyzed sequencing data; AHW, AKHA, AH, MJ, and RWS interpreted data; AHW and AKHA wrote the paper. MJ and RWS performed critical reading and contributed to the writing of the paper.

Compliance with ethical standards

Conflict of interest The authors declare that they have no conflict of interest.

Publisher's note: Springer Nature remains neutral with regard to jurisdictional claims in published maps and institutional affiliations.

Open Access This article is licensed under a Creative Commons Attribution 4.0 International License, which permits use, sharing, adaptation, distribution and reproduction in any medium or format, as long as you give appropriate credit to the original author(s) and the source, provide a link to the Creative Commons license, and indicate if changes were made. The images or other third party material in this article are included in the article's Creative Commons license, unless

indicated otherwise in a credit line to the material. If material is not included in the article's Creative Commons license and your intended use is not permitted by statutory regulation or exceeds the permitted use, you will need to obtain permission directly from the copyright holder. To view a copy of this license, visit <http://creativecommons.org/licenses/by/4.0/>.

References

- Andersson AK, Ma J, Wang J, Chen X, Gedman AL, Dang J, et al. The landscape of somatic mutations in infant MLL-rearranged acute lymphoblastic leukemias. *Nat Genet.* 2015;47:330–7.
- Hyrenius-Wittsten A, Pilheden M, Stureson H, Hansson J, Walsh MP, Song G, et al. De novo activating mutations drive clonal evolution and enhance clonal fitness in *KMT2A*-rearranged leukemia. *Nat Commun.* 2018;9:1770.
- Wei J, Wunderlich M, Fox C, Alvarez S, Cigudosa JC, Wilhelm JS, et al. Microenvironment determines lineage fate in a human model of MLL-AF9 leukemia. *Cancer Cell.* 2008;13:483–95.
- Sontakke P, Carretta M, Jaques J, Brouwers-Vos AZ, Lubbers-Aalders L, Yuan H, et al. Modeling BCR-ABL and MLL-AF9 leukemia in a human bone marrow-like scaffold-based xenograft model. *Leukemia.* 2016;30:2064–73.
- Horton SJ, Jaques J, Woolthuis C, van Dijk J, Mesuraca M, Huls G, et al. MLL-AF9-mediated immortalization of human hematopoietic cells along different lineages changes during ontogeny. *Leukemia.* 2013;27:1116–26.
- Barabé F, Kennedy JA, Hope KJ, Dick JE. Modeling the initiation and progression of human acute leukemia in mice. *Science.* 2007;316:600–4.
- Bailey E, Li L, Duffield AS, Ma HS, Huso DL, Small D. *FLT3/D835Y* mutation knock-in mice display less aggressive disease compared with *FLT3/internal tandem duplication (ITD)* mice. *Proc Natl Acad Sci USA.* 2013;110:21113–8.
- Kikushige Y, Yoshimoto G, Miyamoto T, Ino T, Mori Y, Iwasaki H, et al. Human *Flt3* is expressed at the hematopoietic stem cell and the granulocyte/macrophage progenitor stages to maintain cell survival. *J Immunol.* 2008;180:7358–67.
- Meshinchi S, Alonzo TA, Stirewalt DL, Zwaan M, Zimmerman M, Reinhardt D, et al. Clinical implications of *FLT3* mutations in pediatric AML. *Blood.* 2006;108:3654–61.
- Andersson A, Paulsson K, Lilljebjörn H, Lassen C, Strömbeck B, Heldrup J, et al. *FLT3* mutations in a 10 year consecutive series of 177 childhood acute leukemias and their impact on global gene expression patterns. *Genes Chromosomes Cancer.* 2008;47:64–70.
- Corces MR, Buenrostro JD, Wu B, Greenside PG, Chan SM, Koenig JL, et al. Lineage-specific and single-cell chromatin accessibility charts human hematopoiesis and leukemia evolution. *Nat Genet.* 2016;48:1193–203.
- Lilljebjörn H, Henningsson R, Hyrenius-Wittsten A, Olsson L, Orsmark-Pietras C, Palffy von S, et al. Identification of *ETV6-RUNX1*-like and *DUX4*-rearranged subtypes in paediatric B-cell precursor acute lymphoblastic leukaemia. *Nat Commun.* 2016;7:11790.
- Kim J, Woo AJ, Chu J, Snow JW, Fujiwara Y, Kim CG, et al. A Myc network accounts for similarities between embryonic stem and cancer cell transcription programs. *Cell.* 2010;143:313–24.
- Choudhary C, Schwäble J, Brandts C, Tickenbrock L, Sargin B, Kindler T, et al. AML-associated *Flt3* kinase domain mutations show signal transduction differences compared with *Flt3* ITD mutations. *Blood.* 2005;106:265–73.
- Pratilas CA, Taylor BS, Ye Q, Viale A, Sander C, Solit DB, et al. (V600E)BRAF is associated with disabled feedback inhibition of RAF-MEK signaling and elevated transcriptional output of the pathway. *Proc Natl Acad Sci USA.* 2009;106:4519–24.

Leukemia (2019) 33:2315–2319
<https://doi.org/10.1038/s41375-019-0455-3>

Immunotherapy

Unique CDR3 epitope targeting by CAR-T cells is a viable approach for treating T-cell malignancies

Jinqi Huang^{1,2} · Stepanov Alexey³ · Jian Li⁴ · Terri Jones² · Geramie Grande² · Lacey Douthit² · Jun Xie⁴ · Danna Chen⁵ · Xiaolei Wu⁶ · Maschan Michael⁷ · Changchun Xiao^{4,8} · Jiangning Zhao⁹ · Xuehua Xie¹⁰ · Jia Xie² · Xiao Lei Chen⁴ · Guo Fu⁴ · Gabibov Alexander³ · Chi-Meng Tzeng^{1,11}

Received: 30 July 2018 / Revised: 31 January 2019 / Accepted: 13 March 2019 / Published online: 8 April 2019
 © Springer Nature Limited 2019

To the Editor:

Efficient and specific removal of malignant cells is the ultimate goal of cancer therapy. The current rapid development of chimeric antigen receptor T-cell (CAR-T-cell or CART) therapy potentially provides high efficiency and allows long-term surveillance, which have greatly extended the frontier of leukemia treatment.

T-cell leukemia/lymphoma accounts for 15–25% of the incidence of malignant lymphoid diseases and represents 22 clinicopathologic entities in the most recent classification [1–3]. Recently, researchers have started to investigate approaches using chimeric antigen receptor T-cells (CAR-T-cells or CARTs) to treat T-cell leukemia/lymphoma by targeting common antigens such as CD4, CD5,

TRBC1/2, and the chemokine receptor CCR4 [4–7]. The major hallmark of T-cell leukemia is the clonal expansion of malignant lymphocytes [8–10], which is both a characteristic and diagnostic marker [11, 12]. Given the vast diversity of the immune repertoire, leukemia cell germ-lines from each patient have a unique T-cell receptor (TCR) on the cell surface that distinguishes these cells from normal T-cells. We hypothesized that targeting complementarity-determining region 3 (CDR3) on TCRs on leukemia cells by personalized tumor-specific CARTs would be a valid and superior approach that may offer higher precision and lower off-tumor toxicity than current treatment approaches. Recent advancements in next-generation sequencing (NGS) technology have enabled researchers to investigate TCR diversity with unprecedented depth and efficiency. Here, we propose a novel pipeline based on epitope screening technology aimed at isolating unique CDR3 regions from patients with leukemia/lymphoma for the subsequent redirection of human T-cells toward malignant epitopes. We assumed that the screening of combinatorial single-chain variable fragment

These authors contributed equally: Jinqi Huang, Stepanov Alexey, Jian Li

Supplementary information The online version of this article (<https://doi.org/10.1038/s41375-019-0455-3>) contains supplementary material, which is available to authorized users.

✉ Xiao Lei Chen
Cx12015@xmu.edu.cn

✉ Guo Fu
guofu@xmu.edu.cn

✉ Gabibov Alexander
gabibov@mx.ibch.ru

✉ Chi-Meng Tzeng
cmtzeng@xmu.edu.cn

¹ Translational Medicine Research Center (TMRC), School of Pharmaceutical Sciences, Xiamen University, Xiamen, China

² Department of Chemistry, The Scripps Research Institute, La Jolla, CA 92037, USA

³ M.M. Shemyakin and Yu.A. Ovchinnikov Institute of Bioorganic Chemistry, Russian Academy of Sciences, Miklukho-Maklaya Str., 16 /10, Moscow 117997, Russia

⁴ State Key Laboratory of Cellular Stress Biology, Innovation

Center for Cell Signaling Network, School of Life Sciences, Xiamen University, Xiamen, Fujian, China

⁵ The Affiliated Hospital of Putian University, Putian, Fujian, China

⁶ Present address: ProteinT Biotechnology Ltd. Co. Tianjin Airport Free Trade Zone, Tianjin, China

⁷ Present address: Dmitrii Rogachev Federal Research Center for Pediatric Hematology, Oncology and Immunology, Samory Mashela Str. 1, Moscow 117997, Russia

⁸ Present address: Department of Immunology and Microbiology, The Scripps Research Institute, La Jolla, CA 92037, USA

⁹ Department of Hematology, zhongshan Hospital of Xiamen University, Xiamen 361004 Fujian, China

¹⁰ Department of Oncology, The first hospital of Putian City, Putian 351100 Fujian, China

¹¹ School of Pharmacology, Nanjing Tech University, Nanjing, China

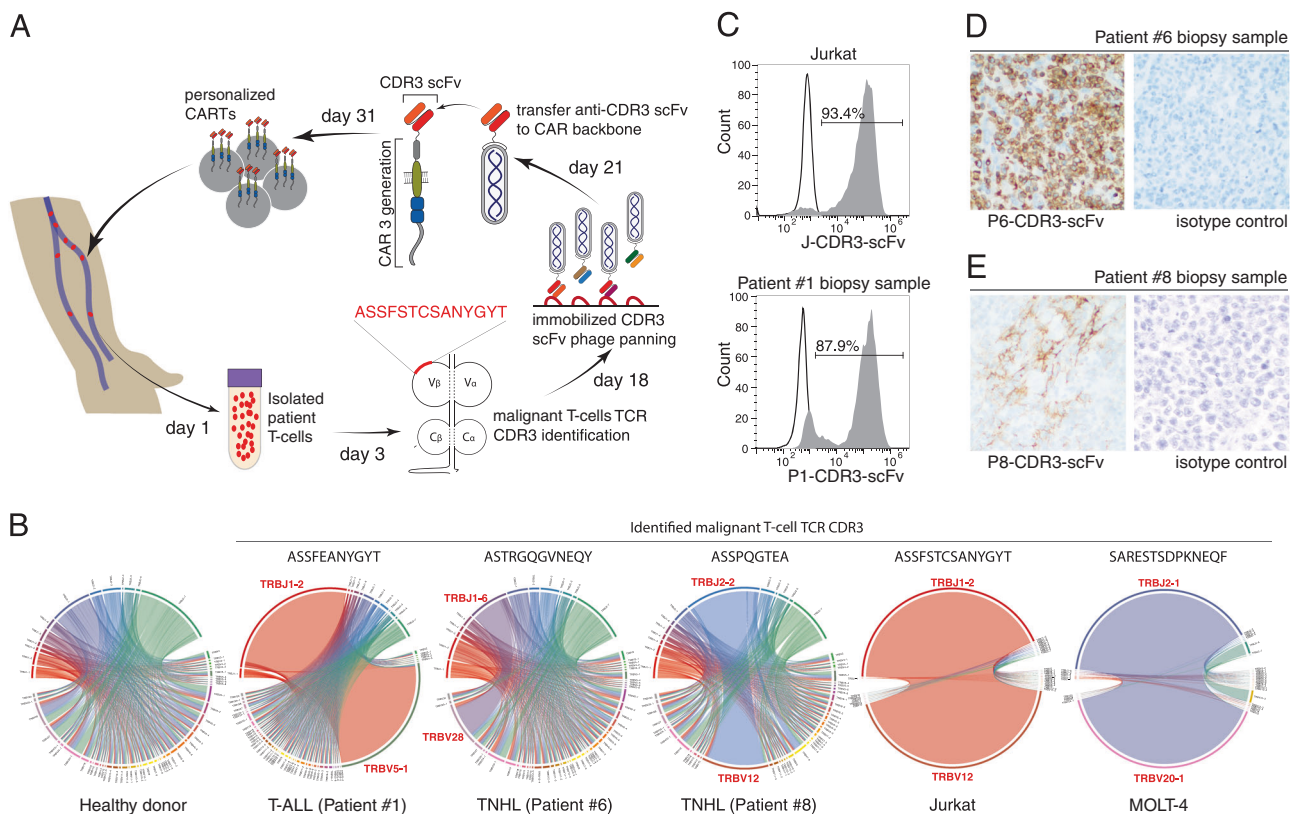


Fig. 1 **a** Workflow for the selection of ligands for personalized CDR3-selective CART therapy for lymphoma and leukemia. A biopsy sample from a patient with lymphoma or leukemia was isolated, and the collected tumor cells were utilized for identification of the TCR CDR3 sequence on malignant T cells. The identified CDR3 sequences were chemically synthesized and used for scFv phage panning. Selected scFv clones were sequenced and transferred to the CAR backbone. Autologous T cells were modified by personalized patient CDR3-selective CARs. **b** NGS analysis of the TCR repertoire from Jurkat, MOLT-4, patient biopsy and healthy donor cells. Representative Circos plots of the frequencies of V β and J β usage and

combinations of unique productive templates. The width of the band is proportional to the frequency. **c** Flow cytometric analysis of Jurkat cells and patient #1 biopsy sample cells stained by GFP fusions of the scFvs specific to the CDR3 regions of the Jurkat cells (J-CDR3-scFv) or Patient#1 malignant T cells (P#1-CDR3-scFv). **d** Immunohistochemistry analysis of the patient#6 biopsy sample stained by GFP fusions of the scFv specific to the CDR3 regions of the Patient#6 malignant T cells (P#6-CDR3-scFv) and isotype antibody control. **e** Immunohistochemistry analysis of the patient#8 biopsy sample stained by GFP fusions of the scFv specific to the CDR3 regions of the Patient#8 malignant T cells (P#6-CDR3-scFv) and isotype antibody control

(scFv) libraries derived from the immune repertoire of cancer patients would allow us to select malignancy-specific epitopes that could facilitate the generation of redirected tumor-specific T-cells. We established a platform spanning from clinical pathology to antigen identification and from targeted scFv screening to in vitro/ in vivo validation, and the entire process can be completed in a relatively short time frame (Fig. 1a). We believe that clonal T-cell CDR3-selective CART therapy is a viable approach for further clinical development, with the potential for extrapolation to B-cell malignancies.

We collected pathological samples from nine leukemia patients (four with T-cell acute lymphoblastic leukemia (T-ALL) and 5 with T-cell non-Hodgkin lymphoma (T-NHL), Supplementary Table S1) pathologically confirmed by histology and flow cytometry, and four healthy donors (normal controls) to study TCR diversity. Isolated cells (as well as Jurkat and MOLT-4 cells as controls) were used for gDNA

extraction, amplification of the CDR3 region of TCR β chain sequences and NGS analysis (Supplementary Fig. S1, Table S2). Consistent with previous reports [13], the TCR diversity of T-cells from leukemia patients showed an abnormal predominance of CDR3 sequences (the frequency ranged from 7 to 94%), while no single clone exhibited a frequency of higher than 2% in T-cells from healthy donors (Fig. 1b). Identified dominant, unique CDR3 sequences from the leukemia, Jurkat and MOLT-4 cells were chemically synthesized and used for further applications.

Seminal studies imply that a patient's immune surveillance system may harbor antibodies against neoepitopes on pathogens or malignant cells [14]. We hypothesized that the antibody library derived from a leukemia patient could be uniquely useful for the selection of antibodies against the patient's malignant TCRs. Therefore, we constructed a phage combinatorial antibody scFv library from 56 patients and 20 healthy donors. Furthermore, we performed phage

display screening of individual peptides. After three rounds of selection, we obtained specific scFvs against CDR3 peptides (Supplementary Table S3). The results of previous structural studies suggest that some CDR3 fragments form rather sophisticated tertiary conformations, which may not be fully represented by chemically synthesized linear peptides. To validate whether our selected antibodies could recognize TCRs harboring the CDR3 sequences, selected scFv-GFP fusion proteins were used to stain the biopsy samples from the patients. The scFv fusion proteins specifically labeled both dispersed cancer cells (Jurkat and patient #1-T-ALL) (Fig. 1c) and lymphoma biopsy (patient #6-peripheral T-cell lymphoma (PTCL) and patient #8-angioimmunoblastic T-cell lymphoma (AITL)) (Fig. 1d, e). To analyze off-target specificity, clinical bone marrow, liver, spleen, and lymph node tissue specimens were stained with selected scFv-GFP fusion proteins. Immunohistochemical examination did not show any detectable off-target binding of the CDR3-specific scFvs (Supplementary Fig. S2). Thus, we concluded that patient B cell repertoire-aided combinatorial antibody library screening is a valid approach to identify antibodies against TCR CDR3 regions on malignant cells for subsequent therapeutic applications.

To explore the possibility of personalized immunotherapy with the CAR approach, the library-selected CDR3-specific scFvs against TCRs on MOLT-4 cells, Jurkat cells, and cells from patient #1 were cloned into lentiviral vectors encoding second-generation CARs and named J-CAR, MOLT-4-CAR and P#1-CAR, respectively. The corresponding lentiviruses were produced and used for transduction of activated primary human T-cells.

We next determined whether T-cells modified with the P#1-CAR and J-CAR constructs exhibited specific cytotoxicity *in vitro*. We incubated CARTs with biopsy cells from patient #1, Jurkat cells or modified Jurkat cells expressing TCRs with the replaced CDR3 from the tumor cells from patient #1 (P1-CDR3-Jurkat). After 24 h of coculture, activated human CDR3-specific T-cells responded to their corresponding Jurkat or patient malignant T-cells by secreting IL-2 and IFN- γ , as well as undergoing highly efficient cell lysis (Fig. 2a).

To validate the specificity of the CARTs targeting CDR3 epitopes on malignant cells, we analyzed the TCR repertoire diversity before and after incubation of the CDR3-selective CARTs or control CART-cells with biopsy cells from patient #1 or Jurkat cells. By ranking the frequency of the V and J regions of the TCRs, we found that control CARTs did not alter the frequency of TCR sequences on malignant cells (Fig. 2b, left panel). However, both J-CARTs and P#1-CARTs drastically reduced the percentage of malignant T-cell clones (Fig. 2b, right panel), suggesting the safety and substantial therapeutic potential of TCR targeting.

The encouraging results described above prompted us to investigate whether this approach could be further validated

in vivo. We tested the efficacy of J-CARTs, MOLT-4-CARTs, and P#1-CARTs in a disseminated leukemia model by *i.v.* engrafting the corresponding target cell lines (Jurkat, MOLT-4 or P1-CDR3-Jurkat cells expressing luciferase) into immunodeficient NOD mice. Two days after tumor inoculation, animals from all experimental groups were treated with CARTs specific to the TCRs on the injected cells or control CARTs with irrelevant CDR3 specificity.

Injection of J-CARTs, MOLT-4-CARTs, and P#1-CARTs significantly reduced the tumor burden in animals and led to cancer cell elimination, while animals injected with control CARTs hosted a progressively increasing number of malignant cells (Fig. 2c). Indeed, compared with animals in the control CART-treated groups, animals in the CDR3-specific groups exhibited improved body weight and extended survival (Fig. 2d).

We demonstrated for the first time that targeting the CDR3 regions of malignant T-cell clones by cell therapy is a viable approach to eliminate leukemia cells. Due to its intrinsic uniqueness, the CDR3 region has historically been an intriguing target with much historical discussion. A few attempts have been made to use this region as the antigen for a cancer vaccine [15]. Due to the clonal nature of leukemia cells and the uniqueness of a given CDR, targeting CDR3 should offer a few advantages not offered by targeting common antigens: (1) Lower “on-target, off-tumor” effect; (2) Minimized impact on a patient’s immune system during treatment; and (3) Great capacity for development as a personalized treatment that can be tailored to individual needs, as a percentage of patients do not respond well to existing therapies with common targets. In the current study, we validated the idea of using CARTs as targeting agents and observed excellent continuous efficacy as well as specificity. Combining CDR3 targeting with the CART approach provides a solution for a substantial portion of patients with T-cell leukemia and lymphoma, with supposedly minimized side effects. The potential problems to be solved in the future include establishing efficient and streamlined good laboratory practice (GLP)-level CDR3 binder discovery and good manufacturing practice (GMP)-level personalized CART manufacturing and decreasing the financial burden for individual patients. However, these issues may be short-lived as technologies develop rapidly.

Nevertheless, after validation of this strategy to eliminate pathological T-cells *ex vivo* and *in vivo*, we envisage this approach as a generally useful alternative and supplement to the popular approach of common antigen targeting to treat T-cell malignancies, especially considering its safety.

Acknowledgements This work was supported by the Fujian Provincial Natural Science Foundation 2016S016 China and Putian city Natural Science Foundation 2014S06(2), Fujian Province, China. Alexey Stepanov and Alexander Gabibov were supported by Russian Scientific Foundation project No. 17-74-30019. Jinqi Huang was supported by a doctoral fellowship from Xiamen University, China.

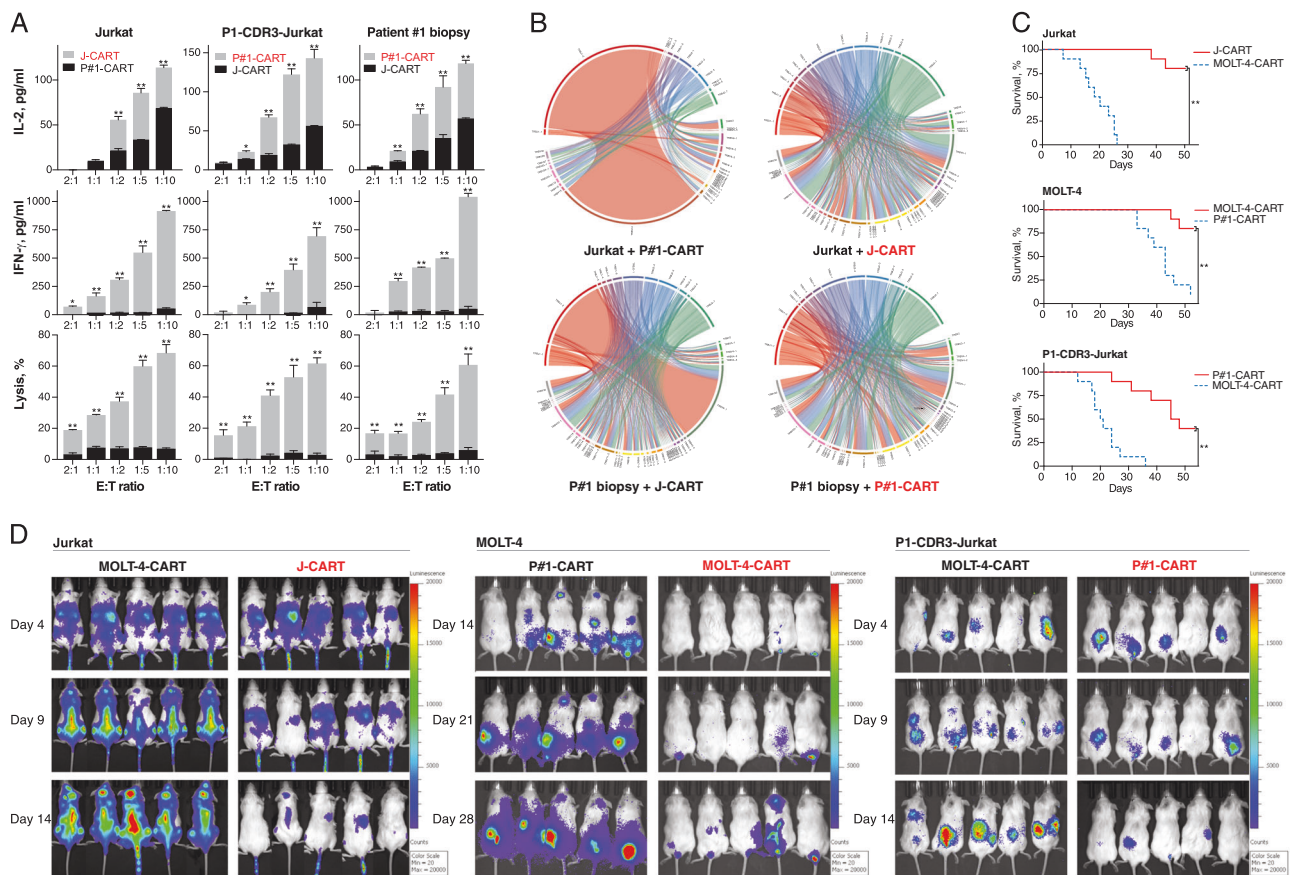


Fig. 2 a P#1-CARTs and J-CARTs were cocultured with biopsy cells from patient #1, Jurkat cells or Jurkat cells with the CDR3 region replaced from malignant cells of patient #1. CARTs with different CDR3 specificities were used for comparison. Cytotoxicity was determined by measuring lactate dehydrogenase release after 6 h. IL-2 and IFN- γ cytokine release was measured after 24 h. All experiments were performed in triplicate wells for each condition and repeated at least twice. **b** TCR repertoire diversity after 24 h of coincubation of

CDR3-selective CARTs or irrelevant CARTs with biopsy cells from patient #1 or Jurkat cells. Survival plots **c** and imaging results **d** for animals inoculated with Jurkat, MOLT-4 or P1-CDR3-Jurkat cells (0.5×10^6 /mouse) and treated by i.v. injection of 5×10^6 CARTs specific to the CDR3 region of the targeted cells or control CARTs ($n = 12$ mice per group). Overall survival curves were plotted using the Kaplan-Meier method and compared using the log-rank (Mantel-Cox) test. Statistical significance: * $p < 0.05$, ** $p < 0.01$

Author Contributions JH, SA, JL, GF, XC, and CMT designed the study; JH, SA, JL, JXJZ, and XX performed and analyzed the experiments; JH, DC, and XW contributed to patient clinical care and data collection; JX and GF provided scientific advice; TJ, GG, and LD proof read the manuscript, JH, SA, JL, GF, MM, AG, JX, and CMT wrote the paper; and all authors read and approved the final version of the manuscript.

Compliance with ethical standards

Conflict of interest: The authors declare that they have no conflict of interest.

Publisher's note: Springer Nature remains neutral with regard to jurisdictional claims in published maps and institutional affiliations.

References

1. Teras LR, DeSantis CE, Cerhan JR, Morton LM, Jemal A, Flowers CR. US lymphoid malignancy statistics by World Health Organization subtypes. *CA Cancer J Clin.* 2016;2016:12.
2. Guru Murthy GS, Dhakal I, Mehta P. Incidence and survival outcomes of chronic myelomonocytic leukemia in the United States. *Leuk Lymphoma.* 2017;58:1648–54.
3. Raetz EA, Teachey DT. T-cell acute lymphoblastic leukemia. *Hematol Am Soc Hematol Educ Program.* 2016;2016:580–8.
4. Pinz KG, Yakoboski E, Jares A, Liu H, Firor AE, Chen KH, et al. Targeting T-cell malignancies using anti-CD4 CAR NK-92 cells. *Oncotarget.* 2017;8:112783–96.
5. Mamonkin M, Rouce RH, Tashiro H, Brenner MK. A T-cell-directed chimeric antigen receptor for the selective treatment of T-cell malignancies. *Blood.* 2015;126:983–92.
6. Maciocia PM, Wawrzyniecka PA, Philip B, Ricciardelli I, Akarca AU, Onuoha SC, et al. Targeting the T-cell receptor beta-chain constant region for immunotherapy of T-cell malignancies. *Nat Med.* 2017;23:1416–23.
7. Perera LP, Zhang M, Nakagawa M, Petrus MN, Maeda M, Kadin ME, et al. Chimeric antigen receptor modified T-cells that target chemokine receptor CCR4 as a therapeutic modality for T-cell malignancies. *Am J Hematol.* 2017;92:892–901.
8. Gong Q, Wang C, Zhang W, Iqbal J, Hu Y, Greiner TC, et al. Assessment of T-cell receptor repertoire and clonal expansion in peripheral T-cell lymphoma using RNA-seq data. *Sci Rep.* 2017;7:11301.

9. Ruggiero E, Nicolay JP, Fronza R, Arens A, Paruzynski A, Nowrouzi A, et al. High-resolution analysis of the human T-cell receptor repertoire. *Nat Commun.* 2015;6:8081.
10. de Leval L, Bisig B, Thielen C, Boniver J, Gaulard P. Molecular classification of T-cell lymphomas. *Crit Rev Oncol Hematol.* 2009;72:125–43.
11. Bertness V, Kirsch I, Hollis G, Johnson B, Bunn PA Jr. T-cell receptor gene rearrangements as clinical markers of human T-cell lymphomas. *N Engl J Med.* 1985;313:534–8.
12. Assaf C, Hummel M, Steinhoff M, Geilen CC, Orawa H, Stein H, et al. Early TCR-beta and TCR-gamma PCR detection of T-cell clonality indicates minimal tumor disease in lymph nodes of cutaneous T-cell lymphoma: diagnostic and prognostic implications. *Blood.* 2005;105:503–10.
13. Wu D, Sherwood A, Fromm JR, Winter SS, Dunsmore KP, Loh ML, et al. High-throughput sequencing detects minimal residual disease in acute T lymphoblastic leukemia. *Sci Transl Med.* 2012;4:134ra163.
14. Yadav M, Delamarre L. IMMUNOTHERAPY. Outsourcing the immune response to cancer. *Science.* 2016;352:1275–6.
15. Iurescia S, Fioretti D, Pierimarchi P, Signori E, Zonfrillo M, Tonon G, et al. Genetic immunization with CDR3-based fusion vaccine confers protection and long-term tumor-free survival in a mouse model of lymphoma. *J Biomed Biotechnol.* 2010;2010:316069.

Leukemia (2019) 33:2319–2323

<https://doi.org/10.1038/s41375-019-0468-y>

Chronic myelogenous leukemia

The phosphatase UBASH3B/Sts-1 is a negative regulator of Bcr-Abl kinase activity and leukemogenesis

Afsar A. Mian^{1,6} · Ines Baumann^{2,7} · Marcus Liebermann³ · Florian Grebien^{2,8} · Giulio Superti-Furga^{2,4} · Martin Ruthardt^{1,3} · Oliver G. Ottmann^{1,3} · Oliver Hantschel^{2,5}

Received: 15 March 2019 / Revised: 20 March 2019 / Accepted: 22 March 2019 / Published online: 8 April 2019

© The Author(s) 2019. This article is published with open access

These authors contributed equally: Afsar A. Mian, Ines Baumann

Joint senior authors of this study: Oliver G. Ottmann, Oliver Hantschel

Supplementary information The online version of this article (<https://doi.org/10.1038/s41375-019-0468-y>) contains supplementary material, which is available to authorized users.

✉ Oliver Hantschel
oliver.hantschel@epfl.ch

¹ Department of Haematology, Division of Cancer and Genetics, School of Medicine, Cardiff University, Cardiff, UK

² CeMM Research Center for Molecular Medicine of the Austrian Academy of Sciences, Vienna, Austria

³ Department of Hematology, Goethe University Frankfurt, Frankfurt/Main, Germany

⁴ Center for Physiology and Pharmacology, Medical University of Vienna, Vienna, Austria

⁵ Swiss Institute for Experimental Cancer Research, School of Life Sciences, École polytechnique fédérale de Lausanne, Lausanne, Switzerland

⁶ Present address: Center for Regenerative Medicine and Stem Cell Research, Aga Khan University, Karachi, Pakistan

⁷ Present address: Department of Pharmacology and Translational Research, Boehringer Ingelheim RCV GmbH & Co KG, Vienna, Austria

⁸ Present address: Institute for Medical Biochemistry, University of Veterinary Medicine Vienna, Vienna, Austria

To the Editor:

The t(9;22) translocation results in the expression of the constitutively active BCR-ABL1 tyrosine kinase. It is detected in chronic myelogenous leukemia (CML) and in ~30% of adult acute lymphoblastic leukemia (ALL) patients [1]. Thus, Ph⁺ ALL is not only the largest genetically defined subgroup of ALL, but also characterized by a poor prognosis [2]. The two major protein isoforms of Bcr-Abl are p210 and p190. Whereas the shorter p190 isoform is specific for Ph⁺ ALL, the longer p210 isoform causes CML, but is also present in ~30% of Ph⁺ ALL patients [1, 3]. BCR-ABL1 was the first oncogene targeted successfully with the tyrosine kinase inhibitor (TKI) imatinib, which results in durable remissions in most CML patients and increased remission rates and survival in Ph⁺ ALL patients. Still, resistance to imatinib occurs particularly frequently in Ph⁺ ALL. Several next-generation TKIs were developed to address TKI resistance and intolerance [4]. Various TKI resistance mechanisms, including dozens of Bcr-Abl mutations, were described, but causes for resistance are still elusive in a significant portion of patients [5].

Deregulation of protein tyrosine phosphatases (PTP) plays an important role in maintaining a wide range of cancers. The ability of tyrosine phosphatases to antagonize

oncogenic tyrosine kinases makes them candidate tumor suppressors. We previously showed that deregulation of PTP1B causes resistance in Ph⁺ leukemias [6]. The phosphatase Sts-1 (suppressor of T-cell receptor signaling 1, encoded by the human UBASH3B gene) was found to be transcriptionally upregulated in Ph⁺ ALL as compared with Ph⁻ ALL patients [7]. Notably, Sts-1 also is one of the most prominent interactors of Bcr-Abl as determined by a systematic interaction proteomics screen [8]. In two recent independent studies, Sts-1 was found to interact more strongly with the Bcr-Abl p210 isoform than with p190 and to be phosphorylated in Bcr-Abl expressing cells [9, 10]. Sts-1 and its only human and mouse paralogue, Sts-2 (UBASH3A), comprise an N-terminal ubiquitin-associated (UBA) domain, an Src homology 3 (SH3) domain and a C-terminal phosphoglycerate mutase (PGM) domain, which has structural homology with the histidine phosphatase superfamily. It was demonstrated that Sts-1 (and to a lesser extent Sts-2) possesses tyrosine phosphatase activity [11]. Strikingly, Sts-1 is a negative regulator of several tyrosine kinase pathways, including not only EGFR and PDGFR, but also ZAP-70 and SYK, thereby antagonizing T- and B-cell receptor signaling, respectively [12, 13]. As genetic and functional perturbation of kinase-phosphatase networks have been implicated in oncogenesis and based on our previous expression and proteomics data, we reasoned that the interaction between the Bcr-Abl kinase and the Sts-1 phosphatase may contribute to leukemogenesis. We therefore investigated the functional relationship between these two proteins, in particular the ability of Sts-1 to dephosphorylate Bcr-Abl and how it may contribute to TKI resistance in Ph⁺ ALL patients.

To study the interaction of Bcr-Abl p190 with Sts-1 and its dependence on kinase activity in Ph⁺ ALL cells, we performed coimmunoprecipitation (co-IP) assays of the endogenous p190 and Sts-1 in Sup-B15 cells either in the absence or presence of imatinib. Sts-1 binding to p190 was largely independent of the Bcr-Abl activation status, as their interaction was only mildly reduced in cells following exposure to imatinib (Fig. 1a). These data were confirmed by co-IP assays using murine Ba/F3 cells stably expressing p190 or Sts-1 as an independent cell-line model. p190 interacted with endogenous or overexpressed Sts-1 regardless of the activation status of Bcr-Abl (Fig. 1b, c).

In order to map the interaction mode of the two proteins, we first determined if Sts-1 binds to the Bcr- or Abl-portion of Bcr-Abl p190. These experiments were performed in Ba/F3 cells upon coexpression of Sts-1 with full-length Bcr-Abl, the Abl-portion (#ABL1) only, the Bcr oligomerization domain directly fused to the Abl-portion (BCC-ABL1) or only the Bcr-portion (BCR; Fig. 1d). These experiments showed that Sts-1 binding was mediated by the Abl-portion of Bcr-Abl, as all Abl-containing constructs, but not the

Bcr-portion alone, bound Sts-1 (Fig. 1d). To map the Sts-1 domains that are required for binding, we performed co-IP assays using loss-of-function point mutations in all domains of Sts-1, including the UBA (W72E), SH3 (W295A), and PGM (H391A) domains (Fig. 1e). To further delineate the requirements for binding to Bcr-Abl, we also assayed these mutants in combination with Bcr-Abl mutants with either abolished kinase activity (Δ K; D382N mutation) or a deletion in the C-terminal last exon region (Δ LE). Sts-1 interacted with the N-terminal part of the Abl-portion of Bcr-Abl encompassing the SH3-SH2-kinase domain unit (Fig. 1e). This interaction was independent of the activation status and the various protein-protein interaction motifs in the C-terminal last exon region of Bcr-Abl. Furthermore, the interaction does not require a functional UBA-, SH3-, or PGM-domain of Sts-1 (Fig. 1e).

To study a possible functional interdependence of the Bcr-Abl/Sts-1 kinase-phosphatase interaction, we first investigated how Sts-1 may regulate Bcr-Abl kinase activity and autophosphorylation at different tyrosine (Y) residues: Y177 in the Bcr-portion is critical for Ras-MAPK signaling, whereas Y245 and Y412 in the Abl-portion are important markers for kinase activation [14]. Thus, we examined the autophosphorylation of Bcr-Abl in Ba/F3 cells in the presence and absence of Sts-1. In line with its binding properties, Sts-1 caused strong dephosphorylation of Bcr-Abl at Abl-Y245 and Abl-Y412, whereas Bcr-Y177 was only mildly dephosphorylated (Fig. 1f). In a second step, we cotransfected HEK293 cells with either Bcr-Abl or an oligomerization-deficient mutant (Δ CC-Bcr-Abl) together with either wild-type or a phosphatase-dead (H391A) Sts-1 [11]. We found that Sts-1 dephosphorylates both Bcr-Abl and itself, and that Sts-1 is a kinase substrate of Bcr-Abl. In fact, Sts-1 dephosphorylated Bcr-Abl and Δ CC-Bcr-Abl strongly and equally well (Fig. 1g). Conversely, only phosphatase-dead Sts-1, but not wild-type Sts-1, was strongly phosphorylated in the presence of Bcr-Abl, demonstrating that Sts-1 is able to dephosphorylate itself (Fig. 1g).

Given that Sts-1 may regulate kinase activity of Bcr-Abl by modulating its autophosphorylation, we next investigated whether Sts-1 impacts on cell proliferation in IL-3-independent Ba/F3 cells expressing wild-type (wt) Bcr-Abl or the gatekeeper mutation T315I, which conveys resistance to multiple TKIs. These cells were retrovirally transduced with GFP or Sts-1-GFP, and proliferation competition assays were performed over the course of 12 days. The expression of GFP alone did not alter the proliferation of BCR-ABL expressing Ba/F3 cells as revealed by the constant percentage of GFP positive cells (Fig. 2a). In contrast, expression of Sts-1-GFP reduced the proliferation of Ba/F3 cells expressing Bcr-Abl wt and T315I. Concomitant treatment with 1 μ M imatinib further decreased proliferation

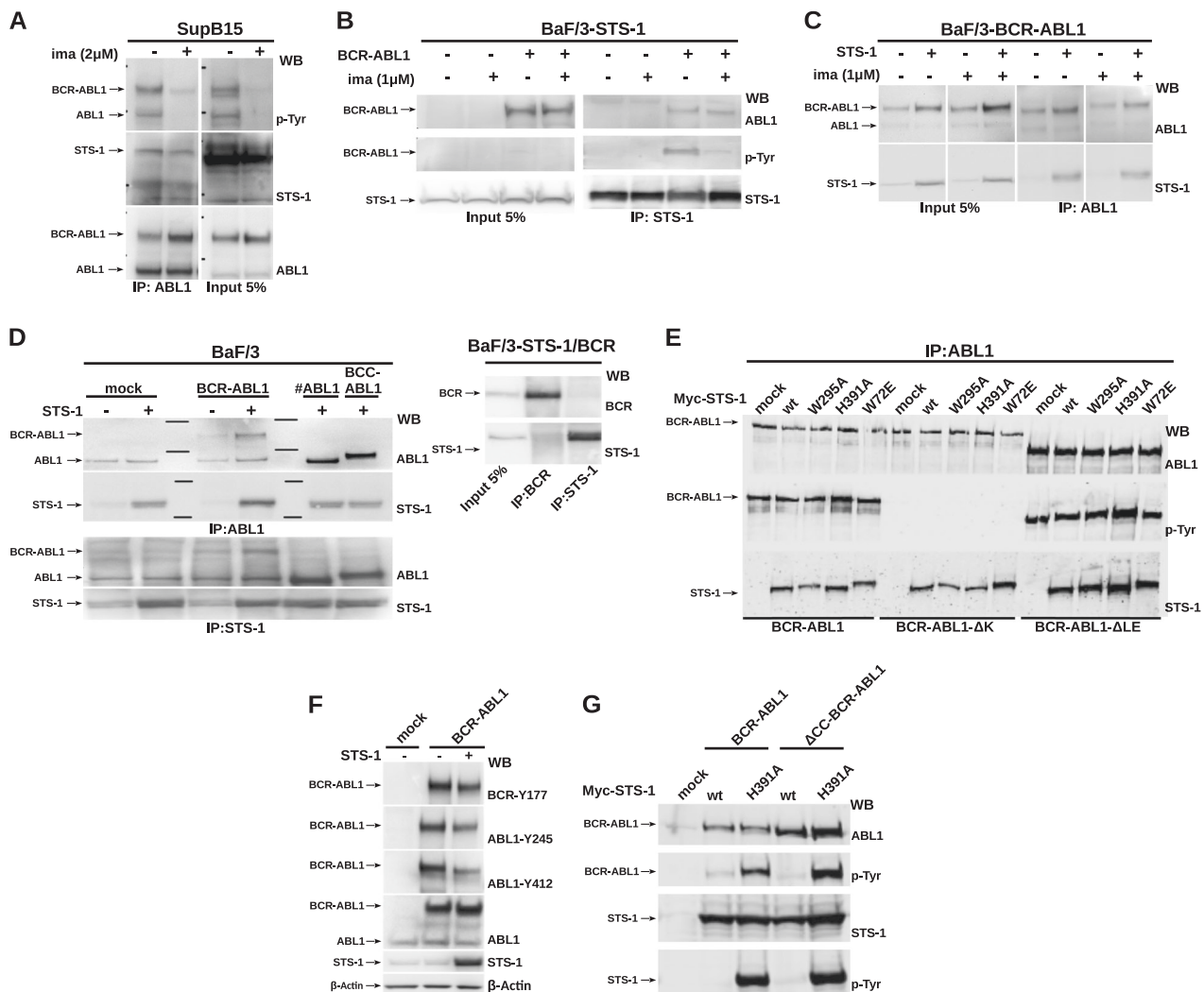


Fig. 1 The Sts-1 phosphatase interacts with and dephosphorylates Bcr-Abl. **a** SupB15 was treated with imatinib (2 μ M for 6 h). ABL1 immunoprecipitates (left panel) from total cell lysates and 5% input fraction (right panel) were immunoblotted with the indicated antibodies. **b** Ba/F3 cells transduced with STS-1 were additionally transduced with BCR-ABL1 and treated with imatinib (1 μ M for 6 h). STS-1 immunoprecipitates (right panel) from total cell lysates and 5% input fraction (left panel) were immunoblotted with the indicated antibodies. **c** Ba/F3 cells transduced with BCR-ABL1 were additionally transduced with STS-1 and treated with imatinib (1 μ M for 6 h). ABL1 immunoprecipitates (right panel) from total cell lysates and 5% input fraction (left panel) were immunoblotted with the indicated antibodies. **d** Ba/F3 cells transduced with full-length Bcr-Abl, the Abl-portion (#ABL1) only, the Bcr oligomerization domain directly fused to the Abl-portion (BCC-ABL1) or only the Bcr-portion (BCR) was additionally transduced with STS-1. ABL1 (upper panels) and STS-1

(lower panels) immunoprecipitates from total cell lysates were immunoblotted with the indicated antibodies. **e** HEK293 cells were cotransfected with BCR-ABL1 wt, Bcr-Abl kinase-dead (D382N; BCR-ABL Δ K) or BCR-ABL1 lacking the C-terminal last exon region (BCR-ABL Δ LE) with STS-1 wt and point mutations in functional domains (UBA (W72E), SH3 (W295A), and PGM (H391A)). ABL1 immunoprecipitates were analyzed by immunoblotting using the indicated antibodies. **f** Ba/F3 cells retrovirally expressing BCR-ABL1 were transfected with STS-1 or empty vector. Whole-cell lysates were then analyzed with the indicated antibodies. **g** HEK293 cells were cotransfected with BCR-ABL1 wt or an oligomerization-defective BCR-ABL1 lacking the coiled-coil domain (Δ CC-BCR-ABL1) with either STS-1 wt or a phosphatase-dead STS-1 mutant (H391A). Total cell lysates were analyzed by immunoblotting using the indicated antibodies

of Bcr-Abl wt, but, as expected, not Bcr-Abl-T315I cells (Fig. 2a). These results indicate that Sts-1 activity negatively regulates cell proliferation induced by Bcr-Abl wt and T315I.

To assess the role of Sts-1 in Bcr-Abl-driven leukemogenesis, we examined the induction of Bcr-Abl p210-

induced CML-like disease in wt vs. Sts-1/Sts-2 double-knockout bone marrow cells using a transduction/transplantation model. The absence of Sts-1/Sts-2 decreased the survival of recipient mice significantly and further aggravated the pronounced splenomegaly observed in mice transplanted with Bcr-Abl-expressing wt cells (Fig. 2b).

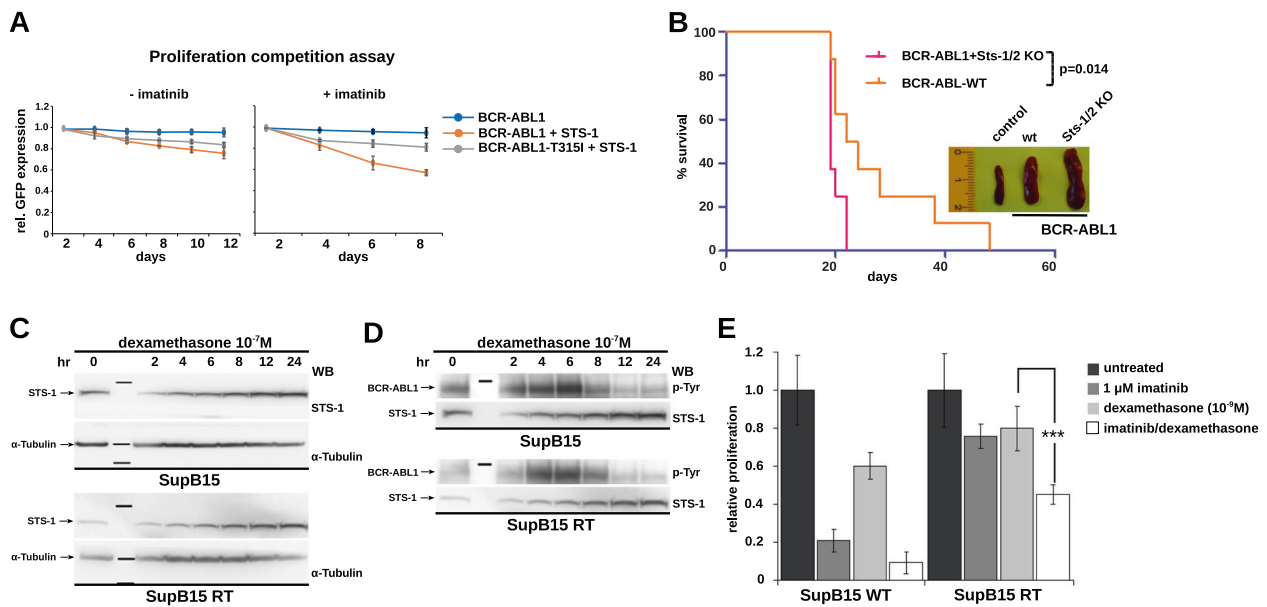


Fig. 2 Sts-1 negatively regulates Bcr-Abl-dependent leukemogenesis and cell proliferation and its expression is upregulated by dexamethasone. **a** The proliferation competition assay with Ba/F3 cell transduced with BCR-ABL1 wt or T315I in the absence or presence of STS-1 expression and without (left) or with (right) imatinib treatment (2 μ M). BCR-ABL1-positive cells are marked with GFP and the relative changes in GFP expression were measured by FACS and followed over time. Mean values \pm SD from three replicates are shown. **b** Equal amounts of primary murine Lin⁻ c-Kit⁺ Sca-1⁺ cells from wt or Sts-1/Sts-2 knockout animals expressing BCR-ABL1 were injected in lethally irradiated recipient mice ($n = 8$ for each group). Overall survival of transplanted mice was monitored over 60 days. P -value = 0.014 was calculated using a logrank (Mantel–Cox) test. Representative spleens from control mice, BCR-ABL1/Sts-1/2 wt and BCR-

ABL1/Sts-1/2 KO mice are shown. **c** SupB15 Ph⁺ ALL cells and their imatinib-resistant subline SupB15RT were exposed to 10^{-7} M dexamethasone, and STS-1 expression was investigated at the given time points. α -Tubulin was used as loading control. **d** SupB15 Ph⁺ ALL cells and their imatinib-resistant subline SupB15RT were exposed to 10^{-7} M dexamethasone, and the effect of increasing expression of STS-1 on BCR-ABL1 phosphorylation was investigated by an anti-p-Tyr antibody. **e** SupB15 and SupB15RT were exposed to imatinib (1 μ M) and 10^{-7} M dexamethasone alone or in combination and proliferation was analyzed by the XTT assay. The bars represent the mean (\pm SEM) of three independent experiments, each performed in triplicates. Statistical significance was calculated using student's t test. *** $p \leq 0.001$

These results indicate that Sts-1/Sts-2 are functionally relevant negative regulators of Bcr-Abl-dependent leukemogenesis in a CML mouse model.

The glucocorticoid dexamethasone and Sts-1 seem to regulate several common signaling pathways: Both inhibit T-cell receptor (TCR) signaling by regulating TCR expression and Sts-1 additionally inhibits certain downstream effectors [15]. In order to harness the therapeutic potential of Sts-1's ability to inhibit growth of Bcr-Abl-positive cells, we explored whether dexamethasone may alter Sts-1 expression and activity. Exposure of Sup-B15 and Sup-B15RT cells to clinically relevant concentrations of dexamethasone increased Sts-1 expression over time, accompanied by decreased Bcr-Abl autophosphorylation in Sup-B15 cells (Fig. 2c, d), indicating that it increases the sensitivity of Bcr-Abl-transformed cells to TKIs. In cell proliferation assays, concomitant treatment with dexamethasone and imatinib showed stronger inhibition than each drug alone in both Sup-B15 and Sup-B15RT cells (Fig. 2e).

Deregulation of the tyrosine phosphatase Sts-1 may be an important and pharmacologically targetable mechanism for Bcr-Abl mutation-independent resistance. Upregulation of Sts-1 in Ph⁺ ALL together with its direct interaction with both p190 and p210 Bcr-Abl strongly suggests a functional deregulation of protein phosphorylation similar to that we previously showed for PTP1B [6]. The fact that its normal function can be restored by ectopic overexpression not only indicates a central role for Sts-1 in the regulation of Bcr-Abl but also that the deregulation of Sts-1 is based on a loss of balance between Bcr-Abl kinase and Sts-1 phosphatase activity. This establishes the upregulation of Sts-1 by drugs, such as dexamethasone, as a valid therapeutic approach for increasing the sensitivity to TKIs.

In conclusion, we delineated the molecular interaction mode of the Sts-1 phosphatase with the Bcr-Abl kinase and provide strong evidence that Sts-1 is a negative regulator of Bcr-Abl signaling, cell proliferation, and leukemogenesis. In addition, the parallel study by Udainiya et al. (submitted) shows a broad impact of Sts-1 on the Bcr-Abl

phosphoproteome network and precisely delineated the Sts-1 interactome using quantitative functional proteomics techniques. Furthermore, we show that modulation of Sts-1 expression by dexamethasone influences TKI sensitivity of Ph⁺ ALL cells. Therefore, the inclusion of dexamethasone for therapy regimens in Ph⁺ ALL for may increase sensitivity to TKIs by upregulating Sts-1.

Acknowledgments This work was supported by the Swiss National Science Foundation (grant 31003A_140913; OH) and the Cancer Research UK Experimental Cancer Medicine Centre Network, Cardiff ECMCI, grant C7838/A15733. We thank N. Carpino for the Sts-1/2 double-KO mice.

Compliance with ethical standards

Conflict of interest The authors declare that they have no conflict of interest.

Publisher's note: Springer Nature remains neutral with regard to jurisdictional claims in published maps and institutional affiliations.

Open Access This article is licensed under a Creative Commons Attribution 4.0 International License, which permits use, sharing, adaptation, distribution and reproduction in any medium or format, as long as you give appropriate credit to the original author(s) and the source, provide a link to the Creative Commons license, and indicate if changes were made. The images or other third party material in this article are included in the article's Creative Commons license, unless indicated otherwise in a credit line to the material. If material is not included in the article's Creative Commons license and your intended use is not permitted by statutory regulation or exceeds the permitted use, you will need to obtain permission directly from the copyright holder. To view a copy of this license, visit <http://creativecommons.org/licenses/by/4.0/>.

References

- Deininger MW, Goldman JM, Melo JV. The molecular biology of chronic myeloid leukemia. *Blood*. 2000;96:3343–56.
- Ottmann OG, Pfeifer H. Management of Philadelphia chromosome-positive acute lymphoblastic leukemia (Ph⁺ ALL). *Hematol Am Soc Hematol Educ Program*. 2009;1:371–81.
- Reckel S, Gehin C, Tardivon D, Georgeon S, Kukenshoner T, Lohr F, et al. Structural and functional dissection of the DH and PH domains of oncogenic Bcr-Abl tyrosine kinase. *Nat Commun*. 2017;8:2101.
- Hantschel O, Grebien F, Superti-Furga G. The growing arsenal of ATP-competitive and allosteric inhibitors of BCR-ABL. *Cancer Res*. 2012;72:4890–5.
- O'Hare T, Zabriskie MS, Eiring AM, Deininger MW. Pushing the limits of targeted therapy in chronic myeloid leukaemia. *Nat Rev Cancer*. 2012;12:513–26.
- Koyama N, Koschmieder S, Tyagi S, Portero-Robles I, Chromic J, Myloch S, et al. Inhibition of phosphotyrosine phosphatase 1B causes resistance in BCR-ABL-positive leukemia cells to the ABL kinase inhibitor STI571. *Clin Cancer Res*. 2006;12:2025–31.
- Juric D, Lacayo NJ, Ramsey MC, Racevskis J, Wiernik PH, Rowe JM, et al. Differential gene expression patterns and interaction networks in BCR-ABL-positive and -negative adult acute lymphoblastic leukemias. *J Clin Oncol*. 2007;25:1341–9.
- Brehme M, Hantschel O, Colinge J, Kaupé I, Planyavsky M, Kocher T, et al. Charting the molecular network of the drug target Bcr-Abl. *Proc Natl Acad Sci USA*. 2009;106:7414–9.
- Reckel S, Hamelin R, Georgeon S, Armand F, Jolliet Q, Chiappe D, et al. Differential signaling networks of Bcr-Abl p210 and p190 kinases in leukemia cells defined by functional proteomics. *Leukemia*. 2017;31:1502–12.
- Cutler JA, Tahir R, Sreenivasamurthy SK, Mitchell C, Renuse S, Nirujogi RS, et al. Differential signaling through p190 and p210 BCR-ABL fusion proteins revealed by interactome and phosphoproteome analysis. *Leukemia*. 2017;31:1513–24.
- Mikhailik A, Ford B, Keller J, Chen Y, Nassar N, Carpino N. A phosphatase activity of Sts-1 contributes to the suppression of TCR signaling. *Mol Cell*. 2007;27:486–97.
- Carpino N, Turner S, Mekala D, Takahashi Y, Zang H, Geiger TL, et al. Regulation of ZAP-70 activation and TCR signaling by two related proteins, Sts-1 and Sts-2. *Immunity*. 2004;20:37–46.
- Raguz J, Wagner S, Dikic I, Hoeller D. Suppressor of T-cell receptor signalling 1 and 2 differentially regulate endocytosis and signalling of receptor tyrosine kinases. *FEBS Lett*. 2007;581:4767–72.
- Hantschel O. Structure, regulation, signaling, and targeting of abl kinases in cancer. *Genes Cancer*. 2012;3:436–46.
- Migliorati G, Bartoli A, Nocentini G, Ronchetti S, Moraca R, Riccardi C. Effect of dexamethasone on T-cell receptor/CD3 expression. *Mol Cell Biochem*. 1997;167:135–44.

Leukemia (2019) 33:2324–2330
<https://doi.org/10.1038/s41375-019-0452-6>

Multiple myeloma gammopathies

Exome sequencing identifies germline variants in *DIS3* in familial multiple myeloma

Maroulio Pertesi^{1,2} · Maxime Vallée¹ · Xiaomu Wei³ · Maria V. Revuelta⁴ · Perrine Galia^{5,6} · Delphine Demangel^{5,6} · Javier Oliver^{1,7} · Matthieu Foll¹ · Siwei Chen³ · Emeline Perrial^{8,9} · Laurent Garderet^{10,11,12} · Jill Corre¹³ · Xavier Leleu¹⁴ · Eileen M. Boyle¹⁵ · Olivier Decaux^{16,17,18} · Philippe Rodon¹⁹ · Brigitte Kolb²⁰ · Borhane Slama²¹ · Philippe Mineur²² · Eric Voog²³ · Catherine Le Bris²⁴ · Jean Fontan²⁵ · Michel Maigre²⁶ · Marie Beaumont²⁷ · Isabelle Azais²⁸ · Hagay Sobol²⁹ · Marguerite Vignon³⁰ · Bruno Royer³⁰ · Aurore Perrot³¹ · Jean-Gabriel Fuzibet³² · Véronique Dorvaux³³ · Bruno Anglaret³⁴ · Pascale Cony-Makhoul³⁵ · Christian Berthou³⁶ · Florence Desquesnes³⁷ · Brigitte Pegourie³⁸ · Serge Leyvraz³⁹ · Laurent Mosser⁴⁰ · Nicole Frenkiel⁴¹ · Karine Augeul-Meunier⁴² · Isabelle Leduc⁴³ · Cécile Leyronnas⁴⁴ · Laurent Voillat⁴⁵ · Philippe Casassus⁴⁶ · Claire Mathiot⁴⁷ · Nathalie Cheron⁴⁸ · Etienne Paubelle⁴⁹ · Philippe Moreau⁵⁰ · Yves-Jean Bignon⁵¹ · Bertrand Joly⁵² · Pascal Bourquard⁵³ · Denis Caillot⁵⁴ · Hervé Naman⁵⁵ · Sophie Rigaudeau⁵⁶ · Gérald Marit⁵⁷ · Margaret Macro⁵⁸ · Isabelle Lambrecht⁵⁹ · Manuel Cliquennois⁶⁰ · Laure Vincent⁶¹ · Philippe Helias⁶² · Hervé Avet-Loiseau⁶³ · Victor Moreno^{64,65} · Rui Manuel Reis^{66,67} · Judit Varkonyi⁶⁸ · Marcin Kruszewski⁶⁹ · Annette Juul Vangsted⁷⁰ · Artur Jurczynski⁷¹ · Jan Maciej Zaucha⁷² · Juan Sainz⁷³ · Malgorzata Krawczyk-Kulis⁷⁴ · Marzena Wątek^{75,76} · Matteo Pelosini⁷⁷ · Elzbieta Iskierka-Jazdzewska⁷⁸ · Norbert Grząsko⁷⁹ · Joaquin Martinez-Lopez⁸⁰ · Andrés Jerez⁸¹ · Daniele Campa⁸² · Gabriele Buda⁷⁶ · Fabienne Lesueur⁸³ · Marek Dudziński⁸⁴ · Ramón García-Sanz⁸⁵ · Arnon Nagler⁸⁶ · Marcin Rymko⁸⁷ · Krzysztof Jamrozak⁷⁵ · Aleksandra Butrym⁸⁸ · Federico Canzian⁸⁹ · Ofure Obazee⁸⁹ · Björn Nilsson² · Robert J. Klein⁹⁰ · Steven M. Lipkin⁴ · James D. McKay¹ · Charles Dumontet^{5,6,8,9}

Received: 5 October 2018 / Revised: 4 February 2019 / Accepted: 8 February 2019 / Published online: 9 April 2019
 © The Author(s) 2019. This article is published with open access

To the Editor:

Multiple myeloma (MM) is the third most common hematological malignancy, after Non-Hodgkin Lymphoma and Leukemia. MM is generally preceded by Monoclonal Gammopathy of Undetermined Significance (MGUS) [1], and epidemiological studies have identified older age, male gender, family history, and MGUS as risk factors for developing MM [2].

The somatic mutational landscape of sporadic MM has been increasingly investigated, aiming to identify recurrent

genetic events involved in myelomagenesis. Whole exome and whole genome sequencing studies have shown that MM is a genetically heterogeneous disease that evolves through accumulation of both clonal and subclonal driver mutations [3] and identified recurrently somatically mutated genes, including *KRAS*, *NRAS*, *FAM46C*, *TP53*, *DIS3*, *BRAF*, *TRAF3*, *CYLD*, *RBI* and *PRDMI* [3–5].

Despite the fact that family-based studies have provided data consistent with an inherited genetic susceptibility to MM compatible with Mendelian transmission [6], the molecular basis of inherited MM predisposition is only partly understood. Genome-Wide Association (GWAS) studies have identified and validated 23 loci significantly associated with an increased risk of developing MM that explain ~16% of heritability [7] and only a subset of familial cases are thought to have a polygenic background [8]. Recent studies have identified rare germline variants predisposing to MM in *KDM1A* [9], *ARID1A* and *USP45* [10], and the implementation of next-generation sequencing technology will allow the characterization of more such rare variants.

In this study, we sought to explore the involvement of rare germline genetic variants in susceptibility to MM.

These authors contributed equally: James D. McKay, Charles Dumontet

Supplementary information The online version of this article (<https://doi.org/10.1038/s41375-019-0452-6>) contains supplementary material, which is available to authorized users.

✉ James D. McKay
 mckayj@iarc.fr

✉ Charles Dumontet
 charles.dumontet@chu-lyon.fr

Extended author information available on the last page of the article

Within our discovery cohort of peripheral blood samples (see Supplementary Methods) from 66 individuals from 23 unrelated families analyzed by WES, *DIS3* (NM_014953) was the only gene in which putative loss-of-function variants were observed in at least two families. An additional cohort of 937 individuals (148 MM, 139 MGUS, 642 unaffected relatives and eight individuals with another hematological condition) from 154 unrelated families (including the individuals in the discovery cohort) were screened for germline variants in *DIS3* using targeted sequencing (Supplementary Table S1). In total, we detected *DIS3* germline putative loss-of-function variants in four unrelated families. The *DIS3* genotypes for the identified variants were concordant between WES and targeted sequencing (where available) and independently confirmed by Sanger sequencing on DNA extracted from uncultured whole blood. The variant allele frequencies (VAF) were close to 50%, as expected of a germline variant (Supplementary figure S1).

The *DIS3* gene, located in 13q22.1, encodes for the catalytic subunit of the human exosome complex, and is recurrently somatically mutated in MM patients [4, 5, 11, 12]. The somatic variants are predominantly missense variants localized in the RNB domain mainly abolishing the exoribonucleolytic activity [4, 13], and are often accompanied by LOH or biallelic inactivation due to 13q14 deletion, implying a tumor suppressor role for *DIS3* in MM [5, 12, 13].

The first *DIS3* variant, observed in 2 affected siblings (1 MGUS and 1 MM case) from family B (Fig. 1a), was located in the splice donor site of exon 13 (c.1755+1G>T; chr13: 73,345,041; GRCh37/hg19, rs769194741) (Supplementary Figure S1a). It is predicted to abolish the splice donor site and cause skipping of exon 13, introducing a premature termination codon (p.Arg557Argfs*3) and result in a truncated *DIS3* protein that lacks part of the exonucleolytic active RNB and S1 domains (Fig. 1b, c). The presence of this variant in two siblings, implying Mendelian segregation, is consistent with a germline, rather than somatic, origin. We investigated whether a *DIS3* transcript from the variant allele is generated but is subsequently eliminated by Nonsense Mediated Decay (NMD) by incubating Lymphoblastoid Cell Lines (LCLs) derived from the two c.1755+1G>T allele carriers with and without puromycin, which suppresses NMD. The mRNA transcript corresponding to the variant allele was clearly present in LCLs treated with puromycin in both carriers, whereas not detectable in untreated LCLs (Fig. 2a), consistent with the variant allele being transcribed but subsequently degraded via the NMD pathway. In line with this observation, analysis of *DIS3* mRNA expression by qRT-PCR showed an average 50% reduced expression in the c.1755+1G>T carriers (range 40.7–61.4%) as compared to non-carriers (Fig. 2b). A second splicing variant (c.1883+1G>C; chr13: 73,342,922; GRCh37/hg19) located in the

splice donor site of exon 14 within the RNB domain was identified in a MM case from family D (Fig. 1a, b, Supplementary figure S1c). However, the individual's mother (Q59), affected with amyloidosis, did not carry the variant, implying that MM in the allele carriers' maternal uncles is unlikely to be explained by this *DIS3* variant. Whether the mRNA transcript encoded by this germline variant undergoes NMD could not be explored due to lack of appropriate material (LCLs, RNA).

A third *DIS3* variant disrupting the wild-type termination codon (stop-loss) (c.2875T>C; p.*959Gln; chr13:73,333,935; GRCh37/hg19, rs141067458) (Fig. 1b, Supplementary Figure S1b) was identified in two unrelated families (A and C, Fig. 1a). This variant is expected to result in a putative read-through variant and a *DIS3* protein with an additional 13 amino acids in the C-terminus (p.*959Glnext*14). It was detected in 3 out of 4 affected siblings (2 MGUS (M63, O53) and 1 MM case (O29)), as well as 5 unaffected relatives (N14, N13, L41, M33 M50) from family A. The Mendelian segregation of this variant in this pedigree is also consistent with germline origin. An additional MM case from family C carried the variant, while we were unable to assess the other MM-afflicted family member (Fig. 1a). As expected of a stop-loss variant, NMD was not observed (data not shown), and gene expression analysis showed no effect on *DIS3* mRNA levels (Fig. 2b). However, western blot analysis demonstrated that *DIS3* protein levels were markedly lower (~50%) in the p.*959Glnext*14 carrier (O53, family A) compared to non-carriers (Fig. 2b, c).

Next, we sought to determine if rare, putative deleterious variants in *DIS3* were more frequent in an independent series of MM cases compared to unaffected individuals. We performed mutation burden tests between 781 MM cases and 3534 controls from the MMRF CoMMpass Study with WES data available. After testing for systemic bias in this dataset (see Supplementary Methods, Supplementary Figure S2), we undertook a burden test for association between functional *DIS3* variants and MM. *DIS3* putative functional variants (truncating and likely deleterious missense variants, see Supplementary Methods) were more frequent among MM patients (30/781) than controls (72/3534) (OR = 1.92 95% CI:1.25–2.96, $p = 0.001$). Although the p.*959Glnext*14 stop-loss variant was recurrently found in 10/781 MM cases and 15/3534 controls (OR = 3.07 95%CI:1.38 to 6.87, $p = 0.0007$), it did not entirely explain the excess of *DIS3* variants among cases as there is evidence for association with other putative functional variants (Supplementary Figure S3a). We additionally genotyped the p.*959Glnext*14 stop-loss variant in an independent series of sporadic MM cases and controls from the IMMEnSE Consortium. While this variant was very rare in this series (8/3020 MM cases relative to 3/1786 controls), there was a consistent but non-significant association between this variant and MM (OR = 3.15 95% CI: 0.74–13.43 $p = 0.122$).

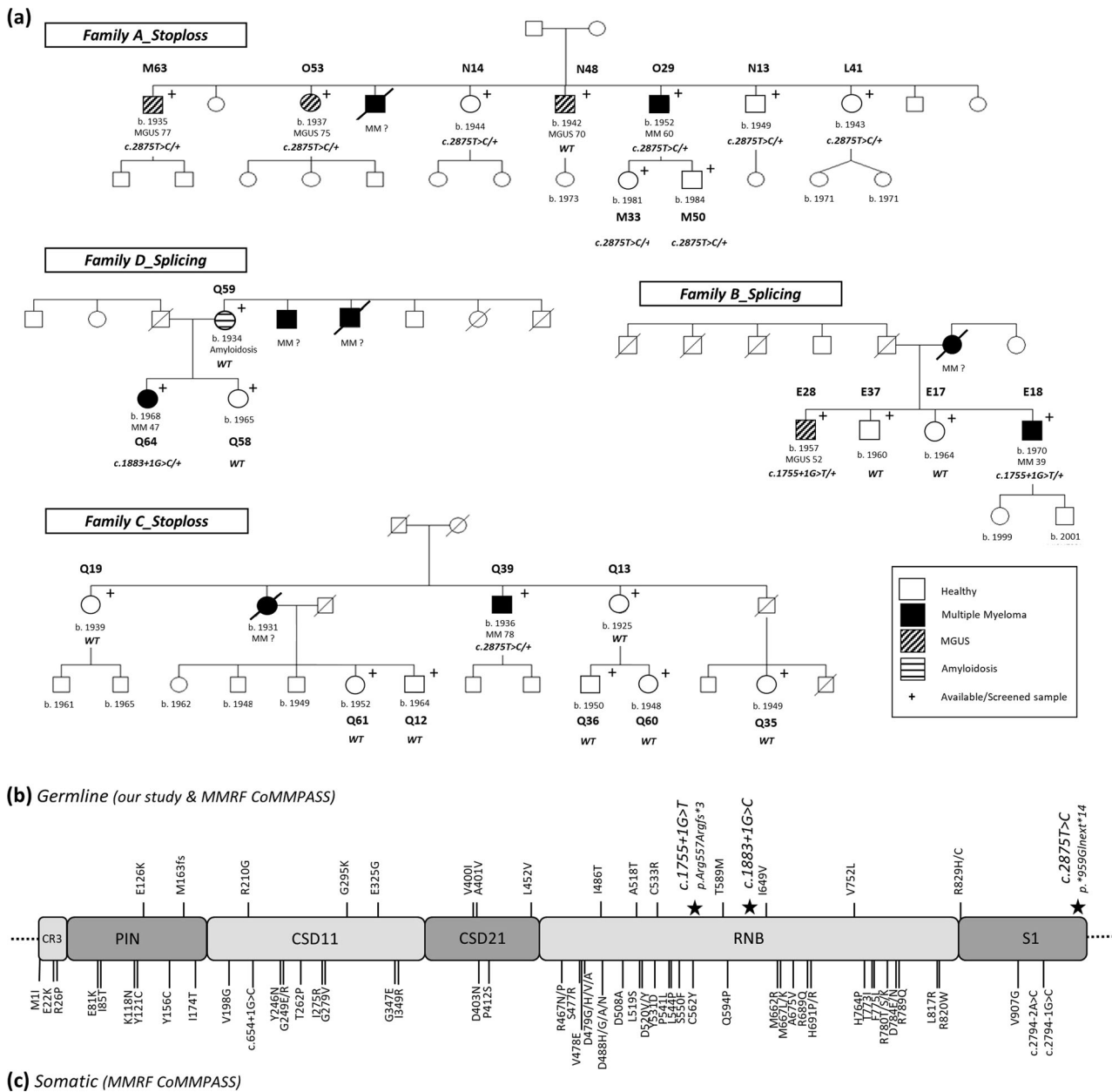


Fig. 1 *DIS3* variants in MM cases. **a** Pedigrees from families carrying a germline *DIS3* variant. Available samples for screening are marked with a “+” symbol. Families A and C carry the p.*959Glnext*14 (c.2875T>C) stop-loss variant. Family B carries the c.1755+1G>T splicing variant and family D carries the c.1883+1G>C splicing variant. The genotype of all screened individuals is shown on each pedigree. WT: wild type. **b**, **c** Schematic representation of identified germline and somatic variants in the distinct *DIS3* protein domains. **b** Germline variants were identified through WES and targeted

resequencing in families with reoccurrence of MM/MGUS as well as in a collection of sporadic MM cases (MMRF CoMMpass Study). The *DIS3* variants discussed in the present study are depicted with a star on the upper part of the figure. **c** Somatic *DIS3* variants were identified in sporadic MM cases from the MMRF CoMMpass Study. We observe that in contrast to the clustering of somatic *DIS3* missense variants in the RNB and PIN domains, germline variants are scattered throughout the gene and consist of splicing, stop-loss and missense variants

To explore the functional consequence of germline *DIS3* variants, we compared MM tumor transcriptomes from patients harboring germline ($n = 21$) and somatic ($n = 96$) *DIS3* putative functional variants to non-carriers ($n = 655$). Differential expression analyses showed an enrichment of pathways associated with global ncRNA processing and translational termination in germline *DIS3* carriers including

ncRNA processing, ncRNA metabolic process, translational termination, and RNA metabolism. Among somatic *DIS3* carriers, significantly enriched pathways include interferon alpha/beta signalling, mRNA splicing, mRNA processing and transcription (Supplementary Figure S3b, Supplementary tables S3 and S4a–d). These findings are consistent with the proposed *DIS3* role in regulating mRNA processing [14] and

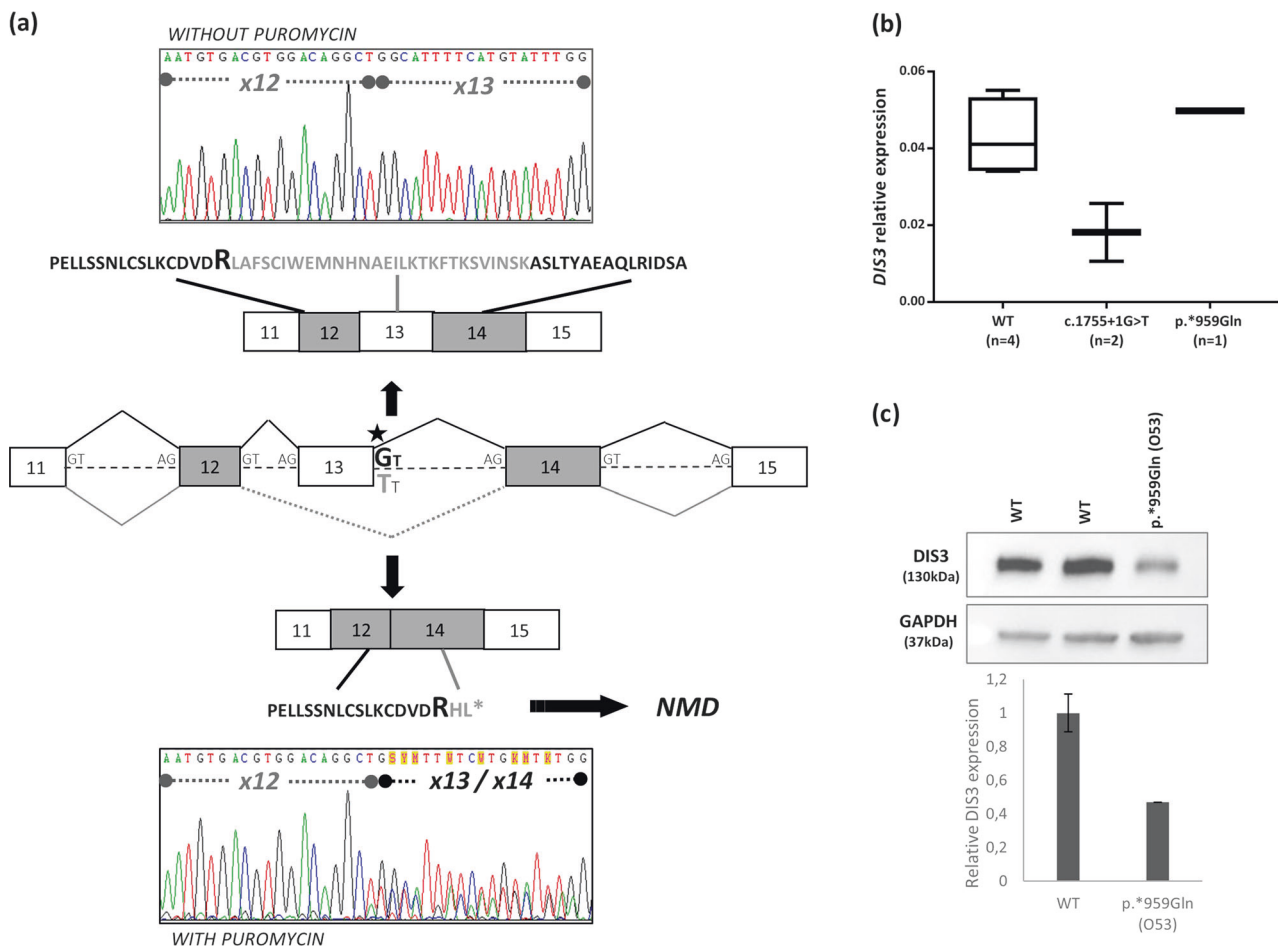


Fig. 2 *DIS3* c.1755+1G>T splicing variant results in nonsense-mediated mRNA decay (NMD) and affects mRNA expression, while the c.2875C>T (p.*959Gln_{next}*14) stop-loss variant affects protein levels. **a** LCLs from patients E18 and E28 (not shown) carrying the c.1755+1G>T splicing variant were cultured with and without puromycin. The chromatogram from treated cells (with puromycin) showed a mixture of the wild-type and mutant transcript lacking exon 13, which was not detected in the non-treated cells (without puromycin). Thus, the mutant transcript is degraded by NMD. **b** Box plot

representing the relative *DIS3* mRNA expression in c.1775+1G>A (n=2) and p.*959Gln_{next}*14 (n=1) carriers compared to non-carriers (n=4). All reactions were performed in triplicates. **c** Western blot with an anti-*DIS3* antibody was performed in LCLs from one p.*959Gln_{next}*14 carrier and two wild-type individuals (anti-GAPDH antibody as internal control). The relative *DIS3* expression in the p.*959Gln_{next}*14 carrier was reduced by 50% compared to non-carriers, suggesting that the mutant allele is translated but degraded shortly after

more specifically mRNA decay, gene expression and small RNA processing [15]. We also observed that, several long-intergenic non-protein coding RNAs, non-coding and anti-sense RNAs were significantly enriched among *DIS3* carriers (Supplementary table S5a, b) supporting previous studies that demonstrate an accumulation of transcripts from non-protein coding regions, snoRNA precursors and certain lncRNAs in *DIS3* mutant cells, along a general deregulation of mRNA levels probably due to the sequestration of transcriptional factors from the accumulated nuclear RNAs [16].

To our knowledge, this is the first observation of germline *DIS3* likely deleterious variants in familial MM and our results suggest that the involvement of *DIS3* in MM etiology may extend beyond somatic alterations to germline susceptibility. We reported rare germline *DIS3* variants in ~2.6% of our cohort of families with multiple cases of MM and MGUS

(4/154). The germline variants described here are predicted to have loss-of-function impact on *DIS3*. Consistent with this, the 1755+1G>T (rs769194741) splicing variant induces NMD and results in reduced *DIS3* mRNA expression, supporting the proposal that *DIS3* is acting as a tumor suppressor gene in MM [13]. Moreover, the c.2875T>C (rs141067458) stop-loss variant (p.*959Gln_{next}*14) results in reduced *DIS3* protein expression suggesting that the mutant allele is translated but degraded shortly after. Notably, in contrast to the clustering of somatic *DIS3* mutations in the PIN and RNB domains, germline variants identified both in familial and sporadic MM cases are scattered throughout the gene (Fig. 1b, c). Despite the fact that these variants do not segregate perfectly with MM in the identified families and the rarity of *DIS3* germline likely deleterious variants limits our statistical power, the subsequent mutation burden and transcriptome

analyses provided supportive data towards *DIS3* acting as an “intermediate-risk” MM susceptibility gene.

Acknowledgements This work was supported by the French National Cancer Institute (INCA) and the Fondation Française pour la Recherche contre le Myélome et les Gammopathies (FFMRG), the Intergroupe Francophone du Myélome (IFM), NCI R01 NCI CA167824 and a generous donation from Matthew Bell. This work was supported in part through the computational resources and staff expertise provided by Scientific Computing at the Icahn School of Medicine at Mount Sinai. Research reported in this paper was supported by the Office of Research Infrastructure of the National Institutes of Health under award number S10OD018522. The content is solely the responsibility of the authors and does not necessarily represent the official views of the National Institutes of Health. The authors thank the Association des Malades du Myélome Multiple (AF3M) for their continued support and participation. Where authors are identified as personnel of the International Agency for Research on Cancer / World Health Organization, the authors alone are responsible for the views expressed in this article and they do not necessarily represent the decisions, policy or views of the International Agency for Research on Cancer / World Health Organization.

Compliance with ethical standards

Conflict of interest The authors declare that they have no conflict of interest.

Publisher’s note: Springer Nature remains neutral with regard to jurisdictional claims in published maps and institutional affiliations.

Open Access This article is licensed under a Creative Commons Attribution 4.0 International License, which permits use, sharing, adaptation, distribution and reproduction in any medium or format, as long as you give appropriate credit to the original author(s) and the source, provide a link to the Creative Commons license, and indicate if changes were made. The images or other third party material in this article are included in the article’s Creative Commons license, unless indicated otherwise in a credit line to the material. If material is not included in the article’s Creative Commons license and your intended use is not permitted by statutory regulation or exceeds the permitted use, you will need to obtain permission directly from the copyright holder. To view a copy of this license, visit <http://creativecommons.org/licenses/by/4.0/>.

References

- Weiss BM, Abadie J, Verma P, Howard RS, Kuehl WM. A monoclonal gammopathy precedes multiple myeloma in most patients. *Blood*. 2009;113:5418–22.
- Morgan GJ, Davies FE, Linet M. Myeloma aetiology and epidemiology. *Biomed Pharmacother*. 2002;56:223–34.
- Bolli N, Avet-Loiseau H, Wedge DC, Van Loo P, Alexandrov LB, Martincorena I, et al. Heterogeneity of genomic evolution and mutational profiles in multiple myeloma. *Nat Commun*. 2014; 5:2997.
- Chapman MA, Lawrence MS, Keats JJ, Cibulskis K, Sougnez C, Schinzel AC, et al. Initial genome sequencing and analysis of multiple myeloma. *Nature*. 2013;471:467–72.
- Lohr JG, Stojanov P, Carter SL, Cruz-Gordillo P, Lawrence MS, Auclair D, et al. Widespread genetic heterogeneity in multiple myeloma: implications for targeted therapy. *Cancer Cell*. 2014; 25:91–101.
- Morgan GJ, Johnson DC, Weinhold N, Goldschmidt H, Landgren O, Lynch HT, et al. Inherited genetic susceptibility to multiple myeloma. *Leukemia*. 2014;28:518–24.
- Went M, Sud A, Försti A, Halvarsson B-M, Weinhold N, Kimber S, et al. Identification of multiple risk loci and regulatory mechanisms influencing susceptibility to multiple myeloma. *Nat Commun*. 2018;9:3707.
- Halvarsson B-M, Wihlborg A-K, Ali M, Lemonakis K, Johnsson E, Niroula A, et al. Direct evidence for a polygenic etiology in familial multiple myeloma. *Blood Adv*. 2017;1:619–23.
- Wei X, Calvo-Vidal MN, Chen S, Wu G, Revuelta MV, Sun J, et al. Germline mutations in lysine specific demethylase 1 (LSD1/KDM1A) confer susceptibility to multiple myeloma. *Cancer research* 2018. <https://doi.org/10.1158/0008-5472.CAN-17-1900>.
- Waller RG, Darlington TM, Wei X, Madsen MJ, Thomas A, Curtin K, et al. Novel pedigree analysis implicates DNA repair and chromatin remodeling in multiple myeloma risk. *PLoS Genet*. 2018;14:e1007111.
- Weißbach S, Langer C, Puppe B, Nedeva T, Bach E, Kull M, et al. The molecular spectrum and clinical impact of *DIS3* mutations in multiple myeloma. *Br J Haematol*. 2015;169:57–70.
- Walker BA, Mavrommatis K, Wardell CP, Ashby TC, Bauer M, Davies FE, et al. Identification of novel mutational drivers reveals oncogene dependencies in multiple myeloma. *Blood* 2018;132:587–97.
- Lionetti M, Barbieri M, Todoerti K, Agnelli L, Fabris S, Tonon G, et al. A compendium of *DIS3* mutations and associated transcriptional signatures in plasma cell dyscrasias. *Oncotarget*. 2015; 6. <https://doi.org/10.18632/oncotarget.4674>.
- Dziembowski A, Lorentzen E, Conti E, Séraphin B. A single subunit, *Dis3*, is essentially responsible for yeast exosome core activity. *Nat Struct Mol Biol*. 2007;14:15–22.
- Robinson S, Oliver A, Chevassut T, Newbury S. The 3’ to 5’ exoribonuclease *DIS3*: from structure and mechanisms to biological functions and role in human disease. *Biomolecules*. 2015;5:1515–39.
- Szczepińska T, Kalisiak K, Tomecki R, Labno A, Borowski LS, Kulinski TM, et al. *DIS3* shapes the RNA polymerase II transcriptome in humans by degrading a variety of unwanted transcripts. *Genome Res*. 2015;25:1622–33.

Maroulio Pertesi^{1,2} · Maxime Vallée¹ · Xiaomu Wei³ · Maria V. Revuelta⁴ · Perrine Galia^{5,6} · Delphine Demangel^{5,6} · Javier Oliver^{1,7} · Matthieu Foll¹ · Siwei Chen³ · Emeline Perriaux^{8,9} · Laurent Garderet^{10,11,12} · Jill Corre¹³ · Xavier Leleu¹⁴ · Eileen M. Boyle¹⁵ · Olivier Decaux^{16,17,18} · Philippe Rodon¹⁹ · Brigitte Kolb²⁰ · Borhane Slama²¹ · Philippe Mineur²² · Eric Voog²³ · Catherine Le Bris²⁴ · Jean Fontan²⁵ · Michel Maignre²⁶ · Marie Beaumont²⁷ · Isabelle Azais²⁸ · Hagay Sobol²⁹ · Marguerite Vignon³⁰ · Bruno Royer³⁰ · Aurore Perrot³¹ · Jean-Gabriel Fuzibet³² · Véronique Dorvaux³³ · Bruno Anglaret³⁴ · Pascale Cony-Makhoul³⁵ · Christian Berthou³⁶ · Florence Desquesnes³⁷ · Brigitte Pegourie³⁸ · Serge Leyvraz³⁹ · Laurent Mosser⁴⁰ · Nicole Frenkiel⁴¹ · Karine Augeul-Meunier⁴² · Isabelle Leduc⁴³ · Cécile Leyronnas⁴⁴ · Laurent Voillat⁴⁵ · Philippe Casassus⁴⁶ · Claire Mathiot⁴⁷ · Nathalie Cheron⁴⁸ · Etienne Paubelle⁴⁹ · Philippe Moreau⁵⁰ · Yves–Jean Bignon⁵¹ · Bertrand Joly⁵² · Pascal Bourquard⁵³ · Denis Caillot⁵⁴ ·

Hervé Naman⁵⁵ · Sophie Rigaudeau⁵⁶ · Gérald Marit⁵⁷ · Margaret Macro⁵⁸ · Isabelle Lambrecht⁵⁹ · Manuel Cliquennois⁶⁰ · Laure Vincent⁶¹ · Philippe Helias⁶² · Hervé Avet-Loiseau⁶³ · Victor Moreno^{64,65} · Rui Manuel Reis^{66,67} · Judit Varkonyi⁶⁸ · Marcin Kruszewski⁶⁹ · Annette Juul Vangsted⁷⁰ · Artur Jurczynszyn⁷¹ · Jan Maciej Zaucha⁷² · Juan Sainz⁷³ · Malgorzata Krawczyk-Kulis⁷⁴ · Marzena Wątek^{75,76} · Matteo Pelosini⁷⁷ · Elzbieta Iskierka-Jażdżewska⁷⁸ · Norbert Grząsko⁷⁹ · Joaquin Martinez-Lopez⁸⁰ · Andrés Jerez⁸¹ · Daniele Campa⁸² · Gabriele Buda⁷⁶ · Fabienne Lesueur⁸³ · Marek Dudziński⁸⁴ · Ramón García-Sanz⁸⁵ · Arnon Nagler⁸⁶ · Marcin Rymko⁸⁷ · Krzysztof Jamrozak⁷⁵ · Aleksandra Butrym⁸⁸ · Federico Canzian⁸⁹ · Ofure Obazee⁸⁹ · Björn Nilsson² · Robert J. Klein⁹⁰ · Steven M. Lipkin⁴ · James D. McKay¹ · Charles Dumontet^{5,6,8,9}


- 1 Genetic Cancer Susceptibility, International Agency for Research on Cancer, Lyon, France
- 2 Department of Laboratory Medicine, Division of Hematology and Transfusion medicine, Lund University, Lund, Sweden
- 3 Biological Statistics and Computational Biology, Cornell University, Ithaca, NY, USA
- 4 Medicine, Weill Cornell Medical College, New York, NY, USA
- 5 ProfilExpert, Lyon, France
- 6 Hospices Civils de Lyon, Lyon, France
- 7 Medical Oncology Service, Hospitales Universitarias Regional y Virgen de la Victoria; Institute of Biomedical Research in Malaga (IBIMA), CIMES, University of Málaga, Málaga, Spain
- 8 INSERM 1052, CNRS 5286, CRCL, Lyon, France
- 9 University of Lyon, Lyon, France
- 10 INSERM, UMR_S 938, Paris, France
- 11 AP-HP, Hôpital Saint Antoine, Département d'hématologie et de thérapie cellulaire, Paris, France
- 12 Sorbonne Universités, UPMC Univ Paris 06, UMR_S 938, Paris, France
- 13 IUC-Oncopole and CRCT INSERM U1037, Toulouse, France
- 14 Inserm CIC 1402 & Service d'Hématologie et Thérapie Cellulaire, CHU La Miletrie, Poitiers, France
- 15 Hôpital Claude Huriez, CHRU, Lille, France
- 16 Service de Medecine Interne, CHU Rennes, Rennes, France
- 17 Faculte de Medecine, Université de Rennes 1, Rennes, France
- 18 INSERM UMR U1236, Rennes, France
- 19 Unite d'Hematologie et d'Oncologie, Centre Hospitalier, Perigueux, France
- 20 Hematologie Clinique, CHU de Reims, Reims, France
- 21 Service d'Onco hematologie, CH Avignon, Avignon, France
- 22 Hematologie et pathologies de la coagulation, Grand Hôpital de Charleroi, Charleroi, Belgium
- 23 Centre Jean Bernard, Institut Inter-regionale de Cancerologie, Le Mans, France
- 24 Service post urgences, CHU de FORT DE FRANCE, pôle RASSUR, Martinique, France
- 25 Hopital Jean Minjoz, CHRU Besançon, Besançon, France
- 26 Service d'Hemato-Oncologie, CHU Chartres, Chartres, France
- 27 Hematologie clinique et therapie cellulaire, CHU Amiens, Amiens, France
- 28 Service de rhumatologie, CHU Poitiers, Poitiers, France
- 29 Cancer Genetics Department, Paoli-Calmettes Institute, Aix-Marseille University, Marseille, France
- 30 Service d'Immuno-hematologie, Hôpital Saint Louis, Paris, France
- 31 Service d'Hematologie, CHU de Nancy, Université de Lorraine, Vandoeuvre les Nancy, Nancy, France
- 32 Internal Medicine Department, Archet Hospital, CHU Nice, Nice, France
- 33 Service d'Hematologie, CHR Mercy, Metz, France
- 34 Unite d'Hematologie, CH Valence, Valence, France
- 35 Service d'Hematologie, Centre Hospitalier Annecy Genevois, Epagny Metz-Tessy, France
- 36 Service d'Hematologie, CHU de Brest, Brest, France
- 37 Haematology Department, CHU UCL Namur, Yvoir, Belgium
- 38 Hematologie clinique, CHU de Grenoble, La Tronche, France
- 39 Departement d'oncologie, CHUV, Lausanne, Switzerland
- 40 Unite d'oncologie medicale, Pôle medical 2, Hôpital Jacques Puel, Rodez, France
- 41 CH Poissy, Saint-Germain-en-Laye, France
- 42 Service Hematologie, Institut de Cancerologie Lucien Neuwirth, Saint-Priest-en-Jarez, France
- 43 Hematologie, CHG Abbeville, Abbeville, France
- 44 Institut Daniel Hollard, Groupe Hospitalier Mutualiste de Grenoble, Grenoble, France
- 45 Service hemato/oncologie, CH William Morey, Chalon sur Saône, France
- 46 Hematologie clinique, Hôpital Avicenne, Bobigny, France
- 47 Intergroupe Francophone du Myelome (IFM), Bobigny, France
- 48 Service Hematologie, CH Bligny, Briis-sous-Forges, France
- 49 Service Hematologie, CH Lyon Sud, Pierre Benite, France
- 50 Service Hematologie, CHU Nantes, Nantes, France
- 51 Laboratoire de Biologie Medicale OncoGènAuvergne;

- Departement d'oncogenetique, UMR INSERM 1240, Centre Jean Perrin, Clermont-Ferrand, France
- 52 Service d'hematologie clinique, Pôle medecine de specialite, Centre Hospitalier Sud Francilien (CHSF), Corbeil-Essonnes, France
- 53 Hematologie Clinique, CHU Nîmes, Nîmes, France
- 54 Hematologie Clinique, CHU Dijon, Dijon, France
- 55 Hematologie - Oncologie medicale, Centre Azureen de Cancerologie, Mougins, France
- 56 Service d'Hematologie et d'Oncologie, CHU de Versailles, Le Chesnay, France
- 57 INSERM U1035, Universite de Bordeaux, Bordeaux, France
- 58 Hematologie Clinique, IHBN-CHU CAEN (University Hospital), Caen, France
- 59 Rheumatology Department, Maison Blanche Hospital, Reims University Hospitals, Reims, France
- 60 Unite d'Hematologie clinique, Groupement des hôpitaux de l'Institut Catholique (GHICL), Universite Catholique de Lille, Lille, France
- 61 Departement d'hematologie clinique, CHU de Montpellier, Montpellier, France
- 62 Service d'Oncologie medicale, CHU de La Guadeloupe, Pointe-a-Pitre, Guadeloupe
- 63 Laboratory for Genomics in Myeloma, Institut Universitaire du Cancer and University Hospital, Centre de Recherche en Cancerologie de Toulouse, Toulouse, France
- 64 CIBER Epidemiología y Salud Pública (CIBERESP), Madrid, Spain
- 65 Unit of Biomarkers and Susceptibility, Cancer Prevention and Control Program, IDIBELL, Catalan Institute of Oncology; Department of Clinical Sciences, Faculty of Medicine, University of Barcelona, Barcelona, Spain
- 66 Life and Health Sciences Research Institute (ICVS), School of Health Sciences, University of Minho, Braga, Portugal; ICVS/3B's-PT Government Associate Laboratory, Braga/Guimarães, Portugal
- 67 Molecular Oncology Research Center, Barretos Cancer Hospital, Barretos, São Paulo, Brazil
- 68 3rd Department of Internal Medicine, Semmelweis University, Budapest, Hungary
- 69 Department of Hematology, University Hospital, Bydgoszcz, Poland
- 70 Department of Haematology, Rigshospitalet, Copenhagen University, Copenhagen, Denmark
- 71 Jagiellonian University Medical College, Department of Hematology, Cracow, Poland
- 72 Gdynia Oncology Center, Gdynia and Department of Oncological Propedeutics, Medical University of Gdańsk, Gdańsk, Poland
- 73 Genomic Oncology Area, GENYO. Centre for Genomics and Oncological Research: Pfizer/University of Granada/Andalusian Regional Government, PTS Granada, Granada, Spain
- 74 Department of Bone Marrow Transplantation and Hematology-Oncology M. Skłodowska-Curie Memorial Cancer Center and Institute of Oncology Gliwice Branch, Gliwice, Poland
- 75 Department of Hematology, Institute of Hematology and Transfusion Medicine, Warsaw, Poland
- 76 Holycross Cancer Center of Kielce, Hematology Clinic, Kielce, Poland
- 77 Department of Oncology, Transplants and Advanced Technologies, Section of Hematology, Pisa University Hospital, Pisa, Italy
- 78 Department of Hematology, Medical University of Lodz, Łódź, Poland
- 79 Department of Experimental Hemato-oncology, Medical University of Lubli, Poland; Department of Hematology, St. John's Cancer Centre, Polish Myeloma Study Group, Lublin, Poland
- 80 Hematology Department, Hospital 12 de Octubre, Universidad Complutense; CNIO, Madrid, Spain
- 81 Hematology and Medical Oncology Department, Hospital Morales Meseguer, IMIB, Murcia, Spain
- 82 Department of Biology, University of Pisa, Pisa, Italy
- 83 Inserm U900, Institut Curie, PSL Research University, Mines ParisTech, Paris, France
- 84 Teaching Hospital No1, Hematology Dept, Rzeszow, Poland
- 85 Hematology Department, University Hospital of Salamanca, IBSAL, Salamanca, Spain
- 86 Hematology Division, Chaim Sheba Medical Center, Tel Hashomer, Israel
- 87 Department of Hematology, Copernicus Hospital, Torun, Poland
- 88 Wroclaw Medical University, Wroclaw, Poland
- 89 Genomic Epidemiology Group, German Cancer Research Center (DKFZ), Heidelberg, Germany
- 90 Department of Genetics and Genomic Sciences and Icahn Institute for Genomics and Multiscale Biology, Icahn School of Medicine at Mount Sinai, New York, NY, USA

Leukemia (2019) 33:2331–2335
<https://doi.org/10.1038/s41375-019-0459-z>

Acute lymphoblastic leukemia

JAK2 p.G571S in B-cell precursor acute lymphoblastic leukemia: a synergizing germline susceptibility

Minhui Lin^{1,2} · Karin Nebral³ · Christoph G. W. Gertzen^{4,5} · Ithamar Ganmore^{6,7,8} · Oskar A. Haas³ · Sanil Bhatia¹ · Ute Fischer¹ · Michaela Kuhlen¹  · Holger Gohlke^{4,5} · Shai Izraeli⁹ · Jan Trka¹⁰ · Jianda Hu² · Arndt Borkhardt¹ · Julia Hauer^{1,11,12} · Franziska Auer^{1,12,13}

Received: 25 September 2018 / Revised: 4 March 2019 / Accepted: 15 March 2019 / Published online: 9 April 2019

© The Author(s) 2019. This article is published with open access

To the Editor:

Germline predispositions are involved in the development of 5% of childhood leukemias [1], although their contribution is believed to be higher. However, to reveal the full spectrum of pathogenic germline variants, individualized genomic patient analyses, in the context of the respective familial background (trio-calling), are needed.

These authors contributed equally as senior authors: Julia Hauer, Franziska Auer

Supplementary information The online version of this article (<https://doi.org/10.1038/s41375-019-0459-z>) contains supplementary material, which is available to authorized users.

✉ Julia Hauer
Julia.Hauer@uniklinikum-dresden.de

✉ Franziska Auer
Franziska.Auer@uniklinikum-dresden.de

¹ Department of Pediatric Oncology, Hematology and Clinical Immunology, Heinrich-Heine University Düsseldorf, Medical Faculty, Düsseldorf, Germany

² Fujian Institute of Hematology, Fujian Provincial Key Laboratory of Hematology, Fujian Medical University Union Hospital, 350001 Fuzhou, Fujian, China

³ Childrens Cancer Research Institute, St. Anna Childrens Hospital, Vienna, Austria

⁴ Institute of Pharmaceutical and Medicinal Chemistry, Heinrich-Heine-Universität Düsseldorf, 40225 Düsseldorf, Germany

⁵ John von Neumann Institute for Computing (NIC), Jülich Supercomputing Centre (JSC) & Institute for Complex Systems - Structural Biochemistry (ICS 6), Forschungszentrum Jülich GmbH, 52425 Jülich, Germany

⁶ Present address: Department of Neurology, Sheba Medical Center, Tel Hashomer, Israel

Here, we present the finding of a germline predisposition to B-cell precursor acute lymphoblastic leukemia (BCP-ALL) that is exerted through two synergizing, separately transmitted germline variants (*JAK2* p.G571S and *STAT3* p.K370R). We demonstrate a modest proliferation potential of *JAK2* p.G571S, which is additionally increased by *STAT3* p.K370R through rewiring of intracellular signaling pathways and show that *JAK2* G571S can rescue a *STAT3* p.K370R-induced cell cycle arrest. Protein modeling of both variants structurally underlines the observed phenotypes. Furthermore, *JAK2* p.G571S could be identified in a second patient with Down syndrome ALL, emphasizing its significance as a recurrent synergizing germline susceptibility variant.

Taken together, we describe *JAK2* p.G571S as a novel germline predisposition in BCP-ALL. Moreover, our data emphasize the synergistic interplay between separately

⁷ Present address: The Joseph Sagol Neuroscience Center, Sheba Medical Center, Tel Hashomer, Israel

⁸ Present address: Sackler Faculty of Medicine, Tel Aviv University, Tel Aviv, Israel

⁹ Division of Pediatric Hematology and Oncology Schneider Children's Medical Center and Tel Aviv University, Tel Aviv, Israel

¹⁰ Pediatric Hematology/Oncology, Childhood Leukemia Investigation Prague, Prague, Czech Republic

¹¹ Department of Pediatrics, Pediatric Hematology and Oncology, University Hospital Carl Gustav Carus, Technische Universität Dresden, Fetscherstrasse 74, 01307 Dresden, Germany

¹² National Center for Tumor Diseases (NCT), Dresden, Germany; German Cancer Research Center (DKFZ), Heidelberg, Germany; Faculty of Medicine and University Hospital Carl Gustav Carus, Technische Universität Dresden, Dresden, Germany; Helmholtz-Zentrum Dresden - Rossendorf (HZDR), Dresden, Germany

¹³ Department of Systems Biology, Beckman Research Institute and City of Hope Comprehensive Cancer Center, Pasadena, CA, USA

transmitted germline risk variants that can render B-cell precursors susceptible to additional somatic hits, allowing BCP-ALL development. Expanding this knowledge is a crucial step towards targeted treatments as well as precision-prevention programs.

Acute lymphoblastic leukemia (ALL) is the most common pediatric cancer (4/100,000) under the age of 15, with the majority of cases affecting B-cell precursors (BCP-ALL) [2]. Although survival rates exceed 90%, it remains a significant cause of death in young children. Thus, to develop novel individualized therapeutic approaches, or even better, to envision precision-prevention programs—in particularly for subtypes of high-risk ALL, elucidation of the tumor genetics are fundamental [3]. In this regard, inherited germline variants are of special interest. Recently, novel germline predisposition syndromes have been described [4], and current studies increasingly highlight the importance of trio-calling analyses in childhood cancer [5, 6].

In this study, we performed trio-calling and describe a novel scenario for lymphoid malignancies, in which two susceptibility loci are inherited—a paternal one and a

maternal one—and both act synergistically in the same signaling pathway, thereby forming a susceptible B-cell precursor compartment that is prone to secondary mutations driving BCP-ALL.

Utilizing whole-exome sequencing we identified two concomitant germline single-nucleotide variants (SNVs) affecting the JAK2/STAT3 pathway in a boy with BCP-ALL (Fig. S1A). The *JAK2* variant, rs139504737 (c.1711G > A), leads to an aminoacid substitution from glycine to serine (p.G571S) and is rarely found within the general population (minor allele frequency (MAF) < 0.01). Interestingly, the same *JAK2* p.G571S germline variant was identified in a Down syndrome (DS-ALL) patient from an independent family (Fig. 1a). The second variant found in the BCP-ALL patient, constitutes an extremely rare, and so far for leukemia undescribed, missense mutation in the *STAT3* gene (c.1109 A > G), causing an exchange of lysine to arginine (p.K370R). While *JAK2* p.G571S was transmitted from the father, *STAT3* p.K370R was inherited from the mother's side (Fig. 1a). Both variants are located in functionally relevant domains, with *STAT3* p.K370R being

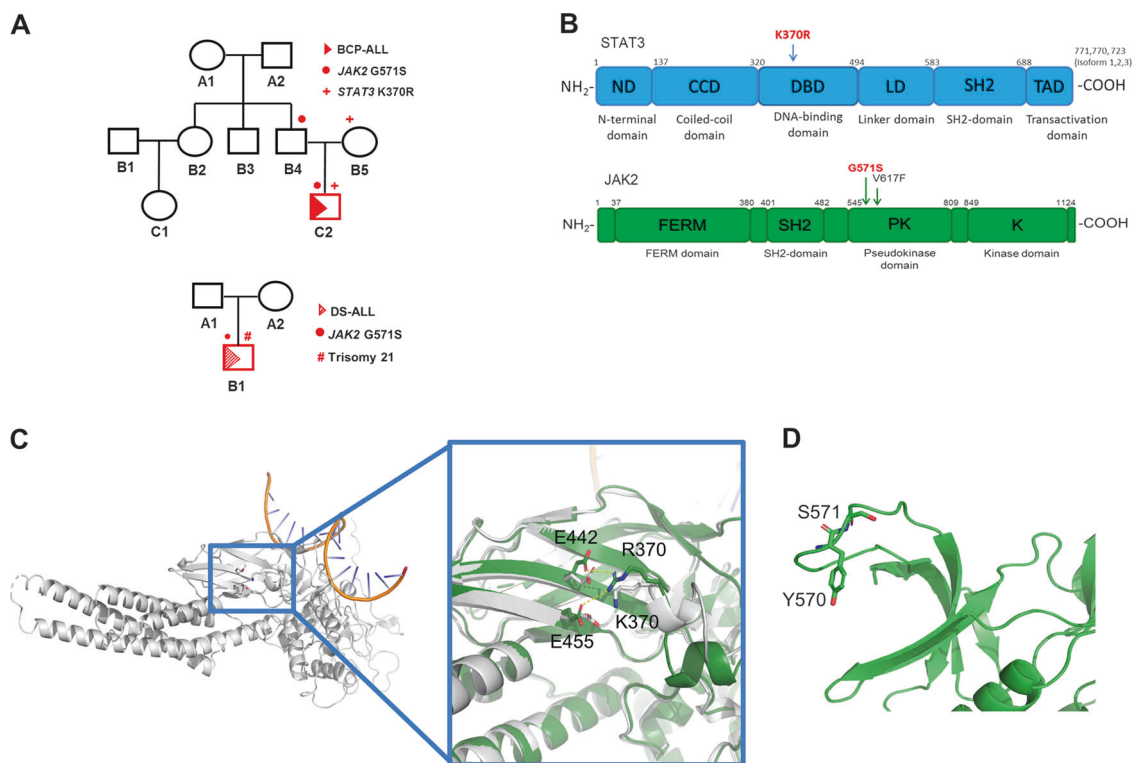


Fig. 1 **a** Pedigree of two independent families harboring *JAK2* p.G571S. The ALL patients are marked with a red triangle, while the transmission of the identified target mutations is highlighted with red symbols (*JAK2* = circle; *STAT3* = +; trisomy 21 = #). **b** Domain organization of *JAK2* and *STAT3* proteins. Identified mutations (red) and the known activating *JAK2* mutation p.V617F (black), which was used as a control, are highlighted. **c** Overview of the *STAT3*-WT (gray) with bound DNA (orange). The blue rectangle indicates the region with the residues of interest (sticks). A close-up depicts the

mutated region in *STAT3*-WT (gray) and the p.K370R variant (dark green). While in the *STAT3*-WT, p.K370 only interacts with p.E455, p.R370 of the p.K370R variant interacts with both p.E442 and p.E455 as indicated by the yellow lines. The mutation of lysine to arginine also distorts the local backbone conformation. **d** Homology model of the p.G571S variant in the *JAK2* protein (green). P.S571 (sticks) is located in a loop between two β -strands next to p.Y570 (sticks), which is one of the most important phosphorylation sites in *JAK2*

localized in the DNA-binding domain and *JAK2* p.G571S in the pseudo-kinase domain, respectively (Fig. 1b).

Furthermore, 11 somatic mutations were identified in the BCP-ALL (Fig. S1B), with a missense mutation in the *CEP89* gene (p.K138T) being the only tumor specific somatic variant. In addition, CytoScanTM-HD analysis revealed loss of *CDKN2A* and *IKZF1* loci, which groups the patient into the recently described *IKZF1*^{plus} subgroup that was shown to have a particularly poor outcome [7] (Fig. S1C). Moreover, a somatic *JAK2* rearrangement was detected by cytogenetic analysis in the second *JAK2* allele. While molecular genetic analysis could rule out a classical *JAK2* fusion with *ETV6*, *BCR*, or *PAX5*, the actual fusion partner was not identified. The patient was enrolled into the AIEOP-BFM 2009 therapy protocol, responded poorly to therapy (prednisone-poor response at day 8, nonremission at day 33) and underwent hematopoietic stem cell transplantation from a matched unrelated donor after achieving first remission (MRD level < 10⁻⁴).

To understand potential phenotypic influences of both mutant proteins on a structural level, we generated homology models of the mutated pseudokinase domain of *JAK2* and the mutated *STAT3*, and compared the models to their respective wild types.

STAT3 p.K370R is located in a loop adjacent to the DNA binding site (Fig. 1c). Moreover, *STAT3* p.K370 is an important site for acetylation, which enables *STAT3*'s interaction with *RELA*, in turn promoting further downstream signaling [8]. In the deacetylated state, *STAT3* p.K370 interacts with p.E455 in a β -sheet. Substitution of lysine to arginine at position p.370 has two implications: first, the arginine can interact with both p.E455 and p.E442 simultaneously, that way strengthening the interaction in the β -sheet. Second, in contrast to lysine, arginine cannot be acetylated. This combination leads to a constitutively non-acetylated form of *STAT3* at position p.370, which was shown to have functional consequences in its interaction capacity with various signaling partners in HEK293T cells [8]. Furthermore, the *STAT3* p.K370R protein did not show an activating phenotype in *STAT3* reporter luciferase assays in HEK293T cells (Fig. S2A). This is in line with the structural modeling, suggesting impaired acetylation rather than phosphorylation (Fig. S2B).

JAK2 p.G571 is located in a 12-residue loop connecting 2 β -strands (Fig. 1d), adjacent to p.Y570, one of the most important phosphorylation sites in *JAK2*. This suggests an influence on the phosphorylation of p.Y570 either through steric hindrance, interactions of the serine sidechain or changes in the backbone conformation near p.Y570. Its unique position affecting amino acid 571, which lies adjacent to the p.Y570 residue that downregulates kinase activity via autophosphorylation hints at a potential

functional mechanism of p.G571S by inhibiting p.Y570-directed negative feedback.

To assess the cooperative potential of both variants, BaF3 depletion assays were carried out. In normal BaF3 cells, neither *STAT3* p.K370R nor *JAK2* p.G571S protein expression alone were sufficient to induce IL-3 independent growth, although immunoblot analyses confirmed increased p-*STAT3* levels in cells expressing both *JAK2* p.G571S and *STAT3* p.K370R (Fig. 2a). Since dimerization by a cytokine receptor facilitates the constitutive activation of *JAK2* mutants, we further transfected BaF3 cells which expressed human *CRLF2* and the *IL7R* alpha chain (leading to the formation of the heterodimeric receptor for thymic stromal lymphopoietin (TSLP) [9]) with the identified target variants. In BaF3/*CRLF2*-*IL-7*WT cells, *JAK2* p.G571S protein expression conferred IL-3 independent growth. Moreover, the combination of both mutant proteins (*JAK2* p.G571S + *STAT3* p.K370R) showed a mild but significant growth advantage starting 2 days after IL-3 withdrawal (Fig. 2b). Immunoblot analysis revealed high-p-AKT levels in cells expressing *JAK2* p.G571S, which was changed to p-*STAT3* through additional expression of *STAT3* p.K370R. Since hyperactivation of p-AKT negatively affects precursor B-cell survival [10], the here observed signal rewiring indicates a synergistic effect of both variants by balancing out signaling strengths.

Besides the cooperating capacity of both identified germline variants, we further observed that the *STAT3* p.K370R mutant protein alone changed the phenotype of the cells in culture, with an accumulation of enlarged BaF3 cells. Surprisingly, this phenotype was reversed in the double mutant cells expressing both *STAT3* p.K370R and *JAK2* p.G571S (Fig. S2C). Cell cycle analysis was in line with this observation, showing a significant increase in >4n cells ($p = 0.0009$), while those in the G-1 phase were significantly decreased ($p = 0.0031$) in *STAT3* p.K370R expressing BaF3 cells compared to *STAT3*-WT cells (Fig. 2c). Again, this phenotype was reduced in BaF3 cells transfected with both mutants simultaneously (G1 phase $p = 0.0026$; >4n, $p = 0.0032$). In line with the reversed cell cycle phenotype in the double mutant cells, immunoblot analysis of the different conditions confirmed increased p-CDC-2, p-CyclinB1/Cyclin-B1, and Cyclin-A2 in BaF3 cells expressing both *JAK2* p.G571S and *STAT3* p.K370R compared to *STAT3* p.K370R alone (Fig. 2c). Taken together, *STAT3* p.K370R conferred a cell cycle arrest in BaF3 cells which is consistent with a loss-of-function phenotype in the *STAT3* reporter luciferase assay and the structural modeling.

These data suggest that the two mutations can act in concert to exert a germline susceptibility toward BCP-ALL development by the accumulation of a susceptible precursor compartment. This compartment might be prone to acquire additional secondary lesions in *IKZF1* and *CDKN2A* or

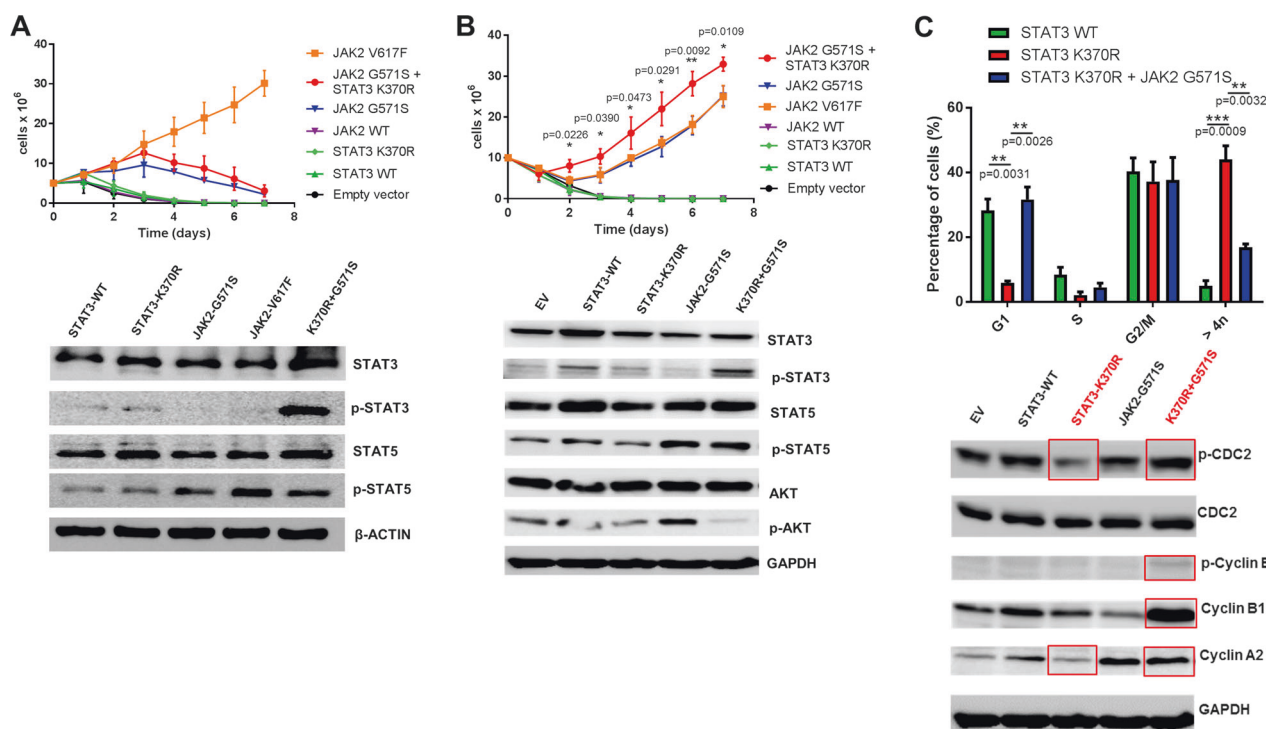


Fig. 2 **a** Top: Proliferation curve showing prolonged survival for BaF3 cells expressing either JAK2 p.G571S protein alone or both JAK2 p.G571S and STAT3 p.K370R proteins. Transfected BaF3 cells were cultured in media without IL-3 for 7 days and their proliferation measured every day using trypan blue. JAK2 p.V617F serves as positive control. Values represent the mean out of three replicates with essentially identical datasets ($n = 3$). Bottom: Immunoblot analysis of BaF3 cells expressing STAT3-WT, STAT3-p.K370R, JAK2-p.G571S, JAK2-p.V617F, or STAT3-p.K370R+JAK2-p.G571S. Depicted are p-STAT3 and p-STAT5 levels of the respective cells. Total STAT3, STAT5, as well as beta-ACTIN serve as loading controls ($n = 2$). **b** Top: Proliferation curve showing prolonged survival for BaF3/CRLF2-IL-7RWT cells expressing either JAK2 p.G571S alone or both JAK2 p.G571S and STAT3 p.K370R. Cells harboring both mutants show a significantly higher proliferation rate compared to cells expressing JAK2 p.G571S, starting at day 2 after IL-3 withdrawal

(calculated by Student's t test: p values are indicated). Cells were cultured as described in (a) ($n = 3$). Bottom: Immunoblot of BaF3/CRLF2-IL-7RWT cells harboring Empty Vector (EV), STAT3-WT, STAT3-p.K370R, JAK2-p.G571S, or STAT3-p.K370R+JAK2-p.G571S expression plasmids. Depicted are p-STAT3, p-STAT5, and p-AKT levels of the respective cells. Total STAT3, STAT5, AKT, as well as GAPDH serve as loading controls ($n = 2$). **c** Top: Cell cycle analysis showing an accumulation of $>4n$, as well as a reduction of cells in the G1-phase for STAT3 p.K370R expressing BaF3 cells, as compared to cells expressing STAT3-WT or STAT3 p.K370R+JAK2 p.G571S. p Values are indicated as calculated by Student's t test ($n = 3$). Bottom: Immunoblot depicting the expression of the cell cycle related proteins CDC2 and Cyclin-B1/B2/A2 in BaF3 cells expressing either EV, STAT3-WT, STAT3-p.K370R, JAK2-p.G571S, or both mutant proteins. GAPDH serves as loading control

alterations of the JAK2 WT allele, which act as somatic oncogenic drivers leading to malignant growth.

Activation of the JAK-STAT pathway is known to be a key event in a variety of hematological malignancies. JAK2 p.V617F leads to constitutively active STAT5 signaling in about 80% of patients suffering from myeloproliferative neoplasms [11], and a high frequency of somatic rearrangements or SNVs activating JAK2 are found in Ph-like ALL [12] and DS-ALL [13, 14]. However, germline JAK2 mutations particularly in BCP-ALL are rare. Here, we identified a second patient harboring germline JAK2 p.G571S in a DS-ALL cohort of 88 patients (Fig. 1a and Fig. S3) [14]. A major proportion of DS-ALL shows high expression of CRLF2 and somatic JAK/STAT pathway activation [15]. Although the analyzed DS-ALL patient did not express a P2RY8-CRLF2 transcript or show a CRLF2

p.232 mutation, he may harbor an activating translocation of CRLF2 into the IGH chain locus. However, due to the lack of patient material we could not test this hypothesis. Therefore, though CRLF2 activation in association with JAK2 p.G571S and trisomy 21 seems highly likely, we cannot confirm an active CRLF2 status in this patient. Nevertheless, the germline JAK2 p.G571S mutation in combination with trisomy 21 can be a complementary scenario of two germline variants acting in synergy to render cells susceptible to additional somatic alterations that can drive ALL development. This insight further strengthens the unique and important role of weak oncogenic germline risk variants (e.g., JAK2 p.G571S) and how they can synergize with additional low-penetrance mutations/alterations to predispose to ALL development.

Thus, we suggest a scenario where *STAT3* p.K370R or trisomy 21 in synergy with *JAK2* p.G571S prime precursor B-cells susceptible for oncogenic transformation through the acquisition of secondary somatic hits. This can be a rational explanation why parents of affected children are healthy throughout life, whereas children who carry both germline variants develop ALL. Increasing knowledge of inherited di-/polygenic variants will be of great importance for the development of novel precision-prevention approaches in the future.

We are indebted to all members of our groups for useful discussions and for their critical reading of the manuscript. Special thanks go to Silke Furlan, Friederike Opitz and Bianca Killing. F.A. is supported by the Deutsche Forschungsgemeinschaft (DFG, AU 525/1-1). J.H. has been supported by the German Children's Cancer Foundation (Translational Oncology Program 70112951), the German Carreras Foundation (DJCLS 02R/2016), Kinderkrebsstiftung (2016/2017) and ERA PerMed GEPARD. Support by Israel Science Foundation, ERA-NET and Science Ministry (SI). A. B. is supported by the German Consortium of Translational Cancer Research, DKTK. We are grateful to the Jülich Supercomputing Centre at the Forschungszentrum Jülich for granting computing time on the supercomputer JURECA (NIC project ID HKF7) and to the "Zentrum für Informations- und Medientechnologie" (ZIM) at the Heinrich Heine University Düsseldorf for providing computational support to H. G. The study was performed in the framework of COST action CA16223 "LEGEND".

Compliance with ethical standards

Conflict of interest The authors declare that they have no conflict of interest.

Publisher's note: Springer Nature remains neutral with regard to jurisdictional claims in published maps and institutional affiliations.

Open Access This article is licensed under a Creative Commons Attribution 4.0 International License, which permits use, sharing, adaptation, distribution and reproduction in any medium or format, as long as you give appropriate credit to the original author(s) and the source, provide a link to the Creative Commons license, and indicate if changes were made. The images or other third party material in this article are included in the article's Creative Commons license, unless indicated otherwise in a credit line to the material. If material is not included in the article's Creative Commons license and your intended use is not permitted by statutory regulation or exceeds the permitted use, you will need to obtain permission directly from the copyright holder. To view a copy of this license, visit <http://creativecommons.org/licenses/by/4.0/>.

References

- Zhang J, Walsh MF, Wu G, Edmonson MN, Gruber TA, Easton J, et al. Germline mutations in predisposition genes in pediatric cancer. *N Engl J Med*. 2015;373:2336–46.
- Mullighan CG. Molecular genetics of B-precursor acute lymphoblastic leukemia. *J Clin Invest*. 2012;122:3407–15.
- Holmfeldt L, Wei L, Diaz-Flores E, Walsh M, Zhang J, Ding L, et al. The genomic landscape of hypodiploid acute lymphoblastic leukemia. *Nat Genet*. 2013;45:242–52.
- Churchman ML, Qian M, Te Kronnie G, Zhang R, Yang W, Zhang H, et al. Germline genetic IKZF1 variation and predisposition to childhood acute lymphoblastic leukemia. *Cancer Cell*. 2018.
- Brozou T, Taeubner J, Velleuer E, Dugas M, Wiczorek D, Borkhardt A, et al. Genetic predisposition in children with cancer—affected families' acceptance of Trio-WES. *Eur J Pediatr*. 2018;177:53–60.
- Kuhlen M, Borkhardt A. Trio sequencing in pediatric cancer and clinical implications. *EMBO Mol Med*. 2018.
- Stanulla M, Dagdan E, Zaliouva M, Moricke A, Palmi C, Cazzaniga G, et al. IKZF1(plus) defines a new minimal residual disease-dependent very-poor prognostic profile in pediatric b-cell precursor acute lymphoblastic leukemia. *J Clin Oncol*. 2018; 36:1240–9.
- Nan J, Hu H, Sun Y, Zhu L, Wang Y, Zhong Z, et al. TNFR2 stimulation promotes mitochondrial fusion via Stat3- and NF- κ B-dependent activation of OPA1 expression. *Circ Res*. 2017;121:392–410.
- Shochat C, Tal N, Bandapalli OR, Palmi C, Ganmore I, te Kronnie G, et al. Gain-of-function mutations in interleukin-7 receptor-alpha (IL7R) in childhood acute lymphoblastic leukemias. *J Exp Med*. 2011;208:901–8.
- Shojaee S, Chan LN, Buchner M, Cazzaniga V, Cosgun KN, Geng H, et al. PTEN opposes negative selection and enables oncogenic transformation of pre-B cells. *Nat Med*. 2016;22:379–87.
- James C, Ugo V, Le Couedic JP, Staerk J, Delhommeau F, Lacout C, et al. A unique clonal JAK2 mutation leading to constitutive signalling causes polycythaemia vera. *Nature*. 2005; 434:1144–8.
- Roberts KG, Li Y, Payne-Turner D, Harvey RC, Yang YL, Pei D, et al. Targetable kinase-activating lesions in Ph-like acute lymphoblastic leukemia. *N Engl J Med*. 2014;371:1005–15.
- Schwartzman O, Savino AM, Gombert M, Palmi C, Cario G, Schrappe M, et al. Suppressors and activators of JAK-STAT signaling at diagnosis and relapse of acute lymphoblastic leukemia in Down syndrome. *Proc Natl Acad Sci USA*. 2017; 114:E4030–e9.
- Bercovich D, Ganmore I, Scott LM, Wainreb G, Birger Y, Elimelech A, et al. Mutations of JAK2 in acute lymphoblastic leukaemias associated with Down's syndrome. *Lancet*. 2008;372:1484–92.
- Izraeli S. The acute lymphoblastic leukemia of Down syndrome—genetics and pathogenesis. *Eur J Med Genet*. 2016;59:158–61.

Leukemia (2019) 33:2336–2340
<https://doi.org/10.1038/s41375-019-0471-3>

Animal models

STAT5B^{N642H} drives transformation of NKT cells: a novel mouse model for CD56⁺ T-LGL leukemia

Klara Klein¹ · Agnieszka Witalisz-Siepracka¹ · Barbara Maurer¹ · Daniela Prinz¹ · Gerwin Heller^{1,2} · Nicoletta Leidenfrost¹ · Michaela Prchal-Murphy¹ · Tobias Suske³ · Richard Moriggi^{3,4,5} · Veronika Sexl¹

Received: 14 November 2018 / Revised: 26 March 2019 / Accepted: 27 March 2019 / Published online: 9 April 2019
 © The Author(s) 2019. This article is published with open access

To the Editor:

The signal transducer and activator of transcription 5B (STAT5B), downstream of IL-15 signaling and Janus kinase (JAK)1, and 3-mediated activation, is a master regulator of development, survival, and function of innate and innate-like lymphocytes (including natural killer (NK) and NKT cells) [1–3]. Gain-of-function mutations in the SH2 domain of human STAT5B, especially STAT5B^{N642H}, are associated with aggressive forms of CD56⁺ T cell (NKT) and NK cell lymphomas/leukemias [4–6]. We described a mouse model expressing human (h)STAT5B^{N642H} under the *Vav-1* promoter, which develops severe CD8⁺ T cell neoplasia [7]. Here, we explore the ability of hSTAT5B^{N642H} to serve as an oncogenic driver in innate lymphocyte neoplasms.

We found an increase in absolute NK cell numbers in the spleen of T cell-diseased hSTAT5B^{N642H} transgenic compared to wild-type (WT) mice (Fig. 1a), despite the relative decrease of the proportion of NK cells among splenic lymphocytes (Fig. S1A), while nonmutant hSTAT5B control mice showed intermediate NK cell numbers (Fig. 1a,

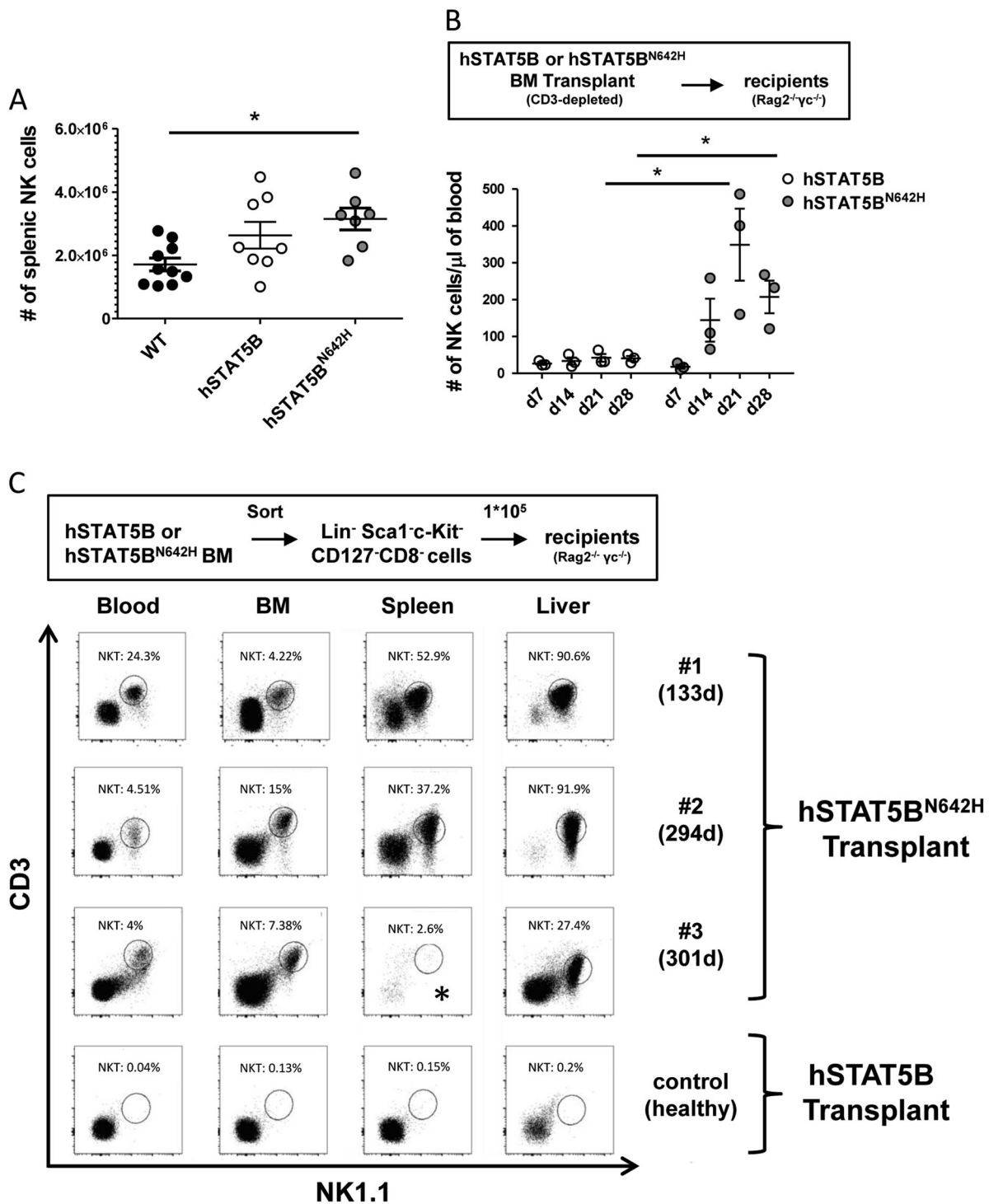
Fig. S1A). No significant differences in NK cell numbers were observed in the bone marrow (BM) between genotypes (Fig. S1B). In addition, both hSTAT5B and hSTAT5B^{N642H} mice showed a similar increase in the proportion of mature NK cells (CD27⁻CD11b⁺ and KLRG1⁺) in the spleen (Fig. S1C, D). These findings suggest that the enforced expression of nonmutant hSTAT5B is sufficient to boost NK cell maturation, which is not further enhanced by introducing the activating hSTAT5B mutation. We hypothesized that any phenotypic alterations affecting innate lymphocytes might be masked by the hSTAT5B^{N642H}-driven aggressive CD8⁺ T cell disease established in hSTAT5B^{N642H} mice at the age of 6–8 weeks [7]. To explore the potential of hSTAT5B^{N642H} to promote NK cell expansion in vivo, we transplanted CD3-depleted BM from hSTAT5B^{N642H} or hSTAT5B mice in immune-deficient Rag2^{-/-}γc^{-/-} recipient mice. Using this approach, we observed an enhanced expansion of NK cells in the blood of hSTAT5B^{N642H} compared to hSTAT5B-transplanted recipients over a time course of 4 weeks (Fig. 1b). Long-term analysis of NK cells in hSTAT5B^{N642H}-transplanted mice was not possible due to expansion of residual CD8⁺ T cells (Fig. S1E, F), which forced us to terminate the experiment. However, after 4 weeks, increased numbers of NK cells were also detected in the spleen upon transplantation of CD3-depleted hSTAT5B^{N642H} compared to hSTAT5B BM (Fig. S1G).

To investigate long-term effects of hSTAT5B^{N642H} on innate lymphocytes, we sorted Lineage (Lin)⁻ (CD3/B220/Ter119/Gr1/CD11b) Sca1⁻c-Kit⁻CD127⁻CD8⁻ cells. This cellular fraction is devoid of hematopoietic stem cells, common lymphoid progenitors, and CD8⁺ T cells and was obtained from hSTAT5B^{N642H} or hSTAT5B BM for further transplantation into Rag2^{-/-}γc^{-/-} recipient mice. We monitored NK and T cell numbers in the blood over a period of 5 weeks. Again, a modest increase but subsequent drop in NK cell numbers in mice transplanted with hSTAT5B^{N642H} compared to hSTAT5B BM cells was observed (Fig. S1H), whereas we failed to detect CD8⁺ T cells in the blood of the

Supplementary information The online version of this article (<https://doi.org/10.1038/s41375-019-0471-3>) contains supplementary material, which is available to authorized users.

✉ Veronika Sexl
 veronika.sexl@vetmeduni.ac.at

- ¹ Institute of Pharmacology and Toxicology, University of Veterinary Medicine Vienna, Vienna, Austria
- ² Department of Medicine I, Medical University of Vienna, Vienna, Austria
- ³ Institute of Animal Breeding and Genetics, University of Veterinary Medicine Vienna, Vienna, Austria
- ⁴ Ludwig Boltzmann Institute for Cancer Research, Vienna, Austria
- ⁵ Medical University of Vienna, Vienna, Austria



recipient animals (Fig. S1I). This indicated that our sorting strategy successfully eliminated CD8⁺ T cell disease, but did not allow us to uncover persistent hSTAT5B^{N642H}-mediated NK cell expansion. Of note, after 4.5–10 months all three hSTAT5B^{N642H}-recipient mice (#1–3) developed a rapidly progressing disease, characterized by expansion of CD3⁺NK1.1⁺ NKT cells in blood, BM, spleen, and liver (Fig. 1c, Table S1). Disease development was restricted to

transplantation of mutant hSTAT5B cells and was not detected upon transplantation of hSTAT5B BM, despite following up these animals for 10 months.

To investigate, whether hSTAT5B^{N642H} NKT cells are indeed transformed and fulfill the criteria of being leukemic, we started to perform serial whole BM transplants from the earlier diseased recipient #1 (survival: 133 d) with the presumably more aggressive disease. To do so,

Fig. 1 hSTAT5B^{N642H} drives limited NK cell expansion and gives rise to leukemia characterized by expansion of NKT cells. **a** Absolute numbers (#) of splenic NK cells (CD3⁻NK1.1⁺NKp46⁺) were determined in WT, hSTAT5B, and hSTAT5B^{N642H} mice by flow cytometry ($n = 10$ (WT), $n = 8$ (hSTAT5B), $n = 7$ (hSTAT5B^{N642H}) pooled from four independent experiments). Symbols represent results from individual mice, horizontal lines indicate mean \pm SEM. * $p < 0.05$, one-way ANOVA. **b** CD3-depleted bone marrow (BM) from hSTAT5B or hSTAT5B^{N642H} mice was transplanted into Rag2^{-/-} γ c^{-/-} recipient mice ($n = 3$) and NK cell numbers were monitored in the blood weekly for 4 weeks by flow cytometry. One representative experiment from two independent experiments is shown. Symbols represent results from individual mice, horizontal lines indicate mean \pm SEM. * $p < 0.05$, unpaired t -test with Welch's correction. **c** Lineage (Lin)⁻ Sca1⁻c-Kit⁻CD127⁻CD8⁻ cells were sorted from BM of hSTAT5B or hSTAT5B^{N642H} mice and 1×10^5 cells were injected into Rag2^{-/-} γ c^{-/-} recipient mice ($n = 3$). Percentages of NKT cells (CD3⁺NK1.1⁺) among living cells in blood, BM, spleen, and liver were analyzed by flow cytometry from the diseased hSTAT5B^{N642H}-transplanted recipient mice (#1–3) (days of survival after transplant are indicated in brackets) and a healthy hSTAT5B-transplanted control mouse. Dot plots are shown. We could not analyze NKT cell frequency in the spleen of mouse #3 (marked by *), due to limited quality of spleen tissue. Analysis was performed when the diseased mice reached the humane endpoint

we transplanted BM containing 1×10^6 NKT cells into immune-deficient Rag2^{-/-} γ c^{-/-} or NSG-recipient mice. This serial transplantation approach was continued for a total of six rounds. The first two rounds were performed to maintain and amplify the NKT cell disease. We confirmed the presence of the hSTAT5B^{N642H} transgene in a diseased mouse (Fig. S1J). Upon the 3rd to the 6th round of serial transplant, we characterized the manifested disease as an aggressive leukemia accompanied by hepatosplenomegaly (Fig. 2a), increased white blood cell (WBC) counts (Fig. S2A) and a high frequency of NKT cells in blood, BM, spleen, and liver (Fig. S2C, D) with a mean survival of 17.6 days (Fig. S2B). Infiltration of leukemic cells into various organs was confirmed by histological analysis (Fig. S2E). In the 6th round, a titration of transplanted NKT cell numbers was performed. Disease severity at the end point was comparable, while a delay of 3 days occurred between each titration step (Fig. 2a, Fig. S2A–D). Despite the increased disease latency in recipients #2 (survival: 294 d) and #3 (survival: 301 d), the disease could also be serially transplanted giving rise to a similarly aggressive disease (Fig. S3A–H) as for recipient #1.

A more detailed characterization of surface markers on transformed NKT cells from the serially transplanted disease of recipient #1 verified expression of the T cell receptor (TCR) β chain, while CD4, CD8, and TCR $\gamma\delta$ expression was not detected. Leukemic cells also stained positive for CD122 and the NK cell markers NKp46 and DX5. No interaction with the CD1d tetramer was observed (Fig. 2b). This surface marker profile corresponds to previously described CD1d-independent NKT cells [8, 9], which were recently identified as a source for CD3⁺NK1.1⁺ T-cell large granular lymphocyte (T-LGL)

leukemia in IL-15 transgenic mice [10]. In analogy to our NKT cell leukemia model, human CD56⁺ T-LGL leukemia cells were also shown to express NKp46 [10]. Additionally, CD3⁺CD56⁺ blasts in human T-LGL leukemia express CD8 [4]. Interestingly, we found CD8 expressed on a subset of hSTAT5B^{N642H} NKT leukemia cells in the two later diseased recipients #2 and #3, but not in recipient #1 (Table S1).

Furthermore, the serially transplanted leukemic NKT cells from recipient #1 were largely negative for activating and inhibitory NK cell receptors, except for Ly49G2 and KLRG1 (Fig. S4A), but stained positive for CD43, CD44, and CD69, while lacking CD62L (Fig. S4A). In summary, this surface receptor expression profile is consistent with an activated phenotype comparable to the leukemic blasts found in IL-15 transgenic mice [11]. The fact that IL-15 transgenic mice develop NK1.1⁺ T-LGL (NKT) or NK cell leukemia [10, 11] supports the importance of the IL-15-STAT5 axis for the transformation of subsets of innate lymphocytes. The occurrence of leukemia with an NKT cell profile in our model suggests that additional IL-15-derived signals, independent of STAT5, may be required for NK cell transformation. In contrast to IL-15 transgenic mice, in which transformation is restricted to innate-like lymphocytes, NKp46⁺ NKT cell disease required the absence of classical CD8⁺ T cells bearing mutant hSTAT5B in vivo. As NKp46⁺ NKT cells represent a minor population [10], the higher number of CD8⁺ T cells may simply outcompete potentially transformed NKT cells. Alternatively, it is possible that CD8⁺ T cells actively suppress the development of NKT cell tumors providing a hostile tumor microenvironment.

hSTAT5B^{N642H}-driven CD8⁺ T cell disease is susceptible to JAK1/JAK2 inhibition by Ruxolitinib treatment [7]. As JAK inhibitors have also been suggested as therapeutic strategy for NK/T-cell lymphoma and aggressive NK cell leukemia [6, 12], we transplanted NSG mice with hSTAT5B^{N642H} NKT leukemia cells and treated them with ruxolitinib for 3 weeks. Treatment attenuated disease severity and decreased hepatosplenomegaly and WBC counts compared to the control group (Fig. 2c and Fig. S4B).

Although initial attempts to grow transformed NKT cells in vitro failed, after 6–8 weeks we detected outgrowth of hSTAT5B^{N642H} NKT cell lines from cultured hepatic leukocytes of three out of nine NSG mice from different serial transplant rounds from recipient #1 (Table S2, Fig. S5A). Two cell lines, derived from the same mouse cultured without or with IL-2 (4165_1 and 4165_2, respectively), were treated with Ruxolitinib and remained sensitive towards it (IC₅₀ of 83 and 72.5 nM, respectively) (Fig. S5B). Furthermore, these cell lines could give rise to leukemia when injected into immune-competent Ly5.1/CD45.1⁺ mice (Fig. S5C–E).

In this study, we identify STAT5B^{N642H} as an oncogenic driver in innate-like lymphocytes. Our novel NKT leukemia

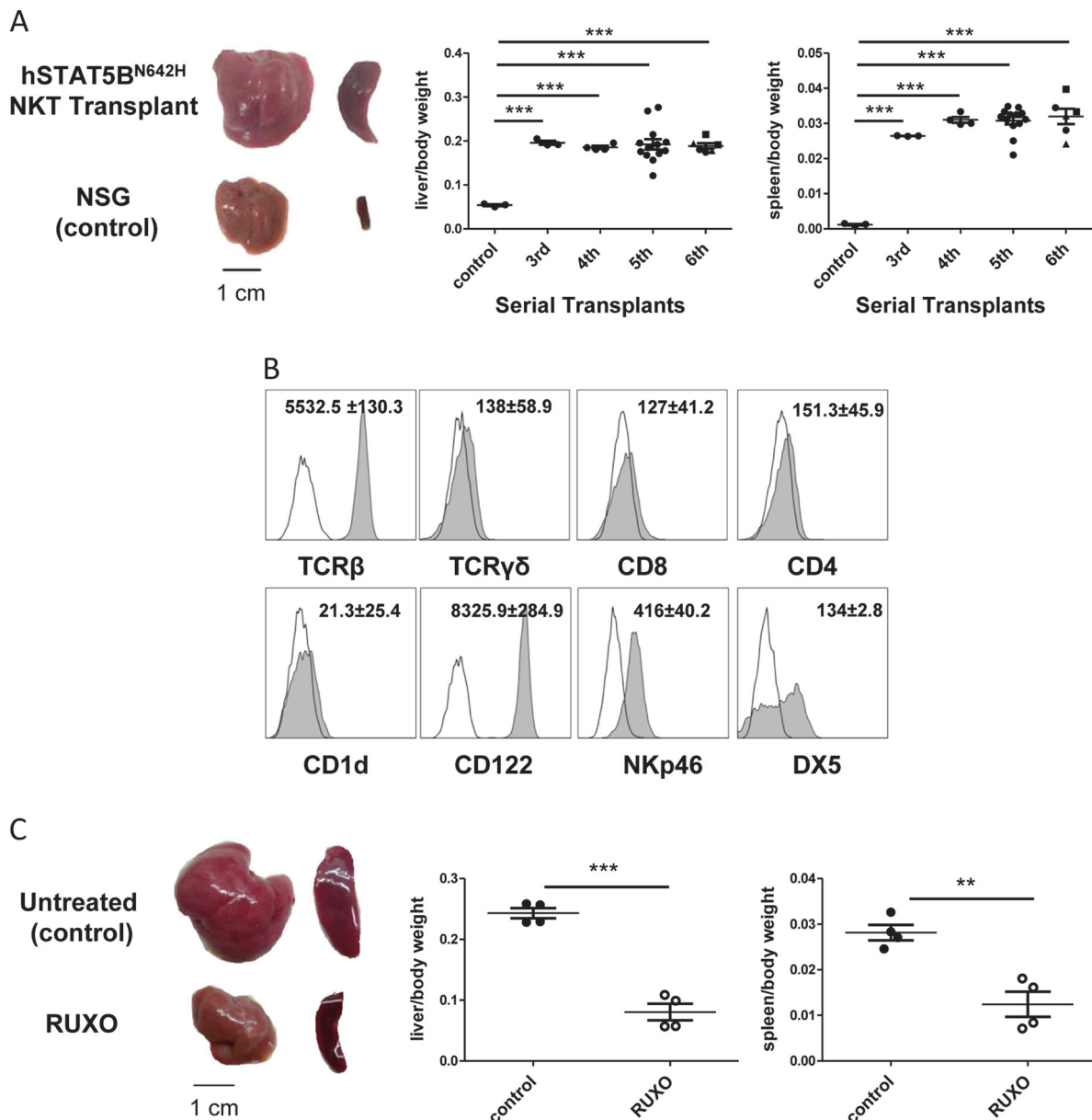


Fig. 2 hSTAT5B^{N642H} induces leukemia of CD1d-independent NKp46⁺ NKT cells, which is serially transplantable and sensitive to Ruxolitinib treatment. **a** BM from NKT cell-diseased recipient #1, transplanted with sorted hSTAT5B^{N642H} BM cells, was serially transplanted into Rag2^{-/-}γc^{-/-} or NSG-recipient mice for six rounds. Whole BM, containing 1×10^6 transformed NKT cells, was transplanted. Of note, in the 6th serial transplant (ST) round a titration of the number of transplanted NKT cells was performed, with two mice each receiving BM containing 1×10^6 (circle), 0.3×10^6 (rectangle), or 0.1×10^6 (triangle) NKT cells. Representative images of liver and spleen from an hSTAT5B^{N642H} NKT cell-transplanted (6th ST) compared to a non-transplanted NSG mouse are shown; line denotes 1 cm (left panel). Relative liver and spleen to body weights are shown for the 3rd to 6th ST ($n = 3$ (3rd ST), $n = 4$ (4th ST), $n = 13$ (5th ST), $n = 6$ (6th ST)) (right panel). Symbols represent results from individual mice, horizontal lines indicate mean \pm SEM. *** $p < 0.001$, unpaired t -test with Welch's correction. **b** Surface marker expression on transformed hSTAT5B^{N642H}

NKT cells was analyzed by flow cytometry. Representative histograms from BM NKT cells of one diseased NSG mouse (4th ST) are shown (unfilled histogram: negative staining control; filled histogram: surface staining). Numbers depict the mean of MFI (median fluorescence intensity, normalized to negative staining control) \pm SEM from three diseased mice (4th ST). **a, b** Analysis was performed when the diseased mice reached the humane endpoint. **c** NSG mice were transplanted with BM containing 1×10^6 hSTAT5B^{N642H} NKT cells (from 5th ST) and treated with Ruxolitinib (RUXO) (85 mg/kg body weight, twice daily) or vehicle control (Nutella[®]) ($n = 4$ per treatment), starting 1 day after NKT cell transplant for 21 days (one experiment). Representative images of liver and spleen to body weights from untreated control and RUXO-treated mice are depicted; line denotes 1 cm (left panel). Relative liver and spleen weights were analyzed in the mice after 3 weeks of treatment (right panel). Symbols represent results from individual mice, horizontal lines indicate mean \pm SEM. ** $p < 0.01$, *** $p < 0.001$, unpaired t -test

model, which is serially transplantable and inducible by frozen material or from cell lines, recapitulates human CD56⁺ LGL leukemia and provides new means for translational research. It will allow a deeper understanding of mechanisms driving NKT leukemia progression and maintenance as well as facilitate finding new therapeutic options. This is of vital importance as the STAT5B^{N642H} mutation in CD56⁺ LGL leukemia patients is associated with a particularly aggressive chemo-refractory phenotype [4].

Acknowledgments We thank Sabine Fajmann and Philipp Jodl for great technical support and Manuela Kindl for maintaining and monitoring the mice.

Funding The work was supported by the Austrian Science Fund FWF grant SFB-F06105 to RM and SFB-F06107 to VS and FWF grant W1212 to VS.

Author contributions VS initiated and supervised the study. KK, AWS, and BM designed the experiments; KK, AWS, BM, DP, and NL performed the experiments; MPM and TS provided technical support; KK and GH analyzed the data; RM provided the mouse model. KK and VS wrote the manuscript. AWS, BM, DP, TS, and RM revised the manuscript.

Compliance with ethical standards

Conflict of interest The authors declare that they have no conflict of interest.

Publisher's note: Springer Nature remains neutral with regard to jurisdictional claims in published maps and institutional affiliations.

Open Access This article is licensed under a Creative Commons Attribution 4.0 International License, which permits use, sharing, adaptation, distribution and reproduction in any medium or format, as long as you give appropriate credit to the original author(s) and the source, provide a link to the Creative Commons license, and indicate if changes were made. The images or other third party material in this article are included in the article's Creative Commons license, unless indicated otherwise in a credit line to the material. If material is not included in the article's Creative Commons license and your intended use is not permitted by statutory regulation or exceeds the permitted use, you will need to obtain permission directly from the copyright holder. To view a copy of this license, visit <http://creativecommons.org/licenses/by/4.0/>.

References

- Eckelhart E, Warsch W, Zebedin E, Simma O, Stoiber D, Kolbe T, et al. A novel Nr1-Cre mouse reveals the essential role of STAT5 for NK-cell survival and development. *Blood*. 2011;117:1565–74.
- Gotthardt D, Sexl V. STATs in NK-cells: the good, the bad, and the ugly. *Front Immunol*. 2017;7:1–8.
- Villarino AV, Sciumè G, Davis FP, Iwata S, Zitti B, Robinson GW, et al. Subset- and tissue-defined STAT5 thresholds control homeostasis and function of innate lymphoid cells. *J Exp Med*. 2017;214:2999–3014.
- Rajala HLM, Eldfors S, Kuusanm H, Van Adrichem AJ, Olson T, Lagstr S, et al. Discovery of somatic STAT5b mutations in large granular lymphocytic leukemia. *Blood*. 2013;121:4541–51.
- Küçük C, Jiang B, Hu X, Zhang W, Chan JKC, Xiao W, et al. Activating mutations of STAT5B and STAT3 in lymphomas derived from $\gamma\delta$ -T or NK cells. *Nat Commun*. 2015;6:6025.
- Dufva O, Kankainen M, Kelkka T, Sekiguchi N, Awad SA, Eldfors S, et al. Aggressive natural killer-cell leukemia mutational landscape and drug profiling highlight JAK-STAT signaling as therapeutic target. *Nat Commun*. 2018;9:1–12.
- Pham HTT, Maurer B, Prchal-Murphy M, Grausenburger R, Grundschober E, Javaheri T, et al. STAT5B N642H is a driver mutation for T cell neoplasia. *J Clin Invest*. 2018;128:387–401.
- Maeda M, Shideo A, Macfadyen AM, Takei F. CD1d-independent NKT cells in β 2 -microglobulin-deficient mice have hybrid phenotype and function of NK and T cells. *J Immunol*. 2004;172:6115–22.
- Farr AR, Wu W, Choi B, Cavalcoli JD, Laouar Y. CD1d-unrestricted NKT cells are endowed with a hybrid function far superior than that of iNKT cells. *Proc Natl Acad Sci USA*. 2014;111:12841–6.
- Yu J, Tridandapani S, Caligiuri MA, Yu J, Mitsui T, Wei M, et al. Nkp46 identifies an NKT cell subset susceptible to leukemic transformation in mouse and human. *J Clin Invest*. 2011;121:1456–70.
- Yokohama A, Mishra A, Mitsui T, Becknell B, Johns J, Curphey D, et al. A novel mouse model for the aggressive variant of NK cell and T cell large granular lymphocyte leukemia. *Leuk Res*. 2010;34:1–14.
- Hee YT, Yan J, Nizetic D, Chng W. LEE011 and ruxolitinib: a synergistic drug combination for natural killer/T-cell lymphoma (NKTCL). *Oncotarget*. 2018;9:31832–41.